



CTF3-Note-101

**Comprehensive user manual for the phase-coding
system setup and operation with PHIN including the
measurements performed with the beam.**

By

Marta 'Csatari' Divall,

A. Andersson, B. Bolzon, E. Bravin, E. Chevallay, S. Döbert,

A. Drozdy, V. Fedosseev, C. Hessler, T. Lefèvre,

S. Livesley, Ö. Mete, M. Olvegaard, A.N. Rabiller

Contents

1. Introduction
 - 1.1. Advantage of laser based phase-coding
 - 1.2. Requirements/specification/precision
2. Design choice
 - 2.1. Pockels-cell option at high power
 - 2.2. Fiber optic polarization switch
 - 2.3. Fiber modulator solution
 - 2.3.1. Initial tests/ one modulator scheme
 - 2.3.2. Two modulator scheme
3. System setup
 - 3.1. Online amplitude and phase adjustment
 - 3.1.1. The frequency domain method
 - 3.1.2. The time domain method
 - 3.1.3. Comparison of accuracy between the two methods
 - 3.2. Components
 - 3.2.1. Coupling into the fiber
 - 3.2.2. The 50/50 splitter/ combiner from Photline
 - 3.2.3. Modulators
 - 3.2.4. Delay line
 - 3.2.5. Attenuator
 - 3.3. Assembly
 - 3.3.1. Fiber input set up to the Thorlabs Nanomax stage
 - 3.3.2. Delay setup
 - 3.3.3. Modulator transmission setup
 - 3.3.4. Driver setup
 - 3.3.5. Final adjustment
4. Integration into the laser chain
 - 4.1. Fiber amplifier
 - 4.2. Beam profile and stability
 - 4.3. Full amplification/ Harmonics
 - 4.4. Timing signals for the phase-coding
5. Measurements with phase-coding
 - 5.1. Measurements on the laser
 - 5.1.1. Timing and amplitude accuracy
 - 5.1.2. Satellite measurements
 - 5.2. Measurements on PHIN
 - 5.2.1. Cherenkov-line measurements
 - 5.2.2. FCT measurements
 - 5.2.3. Energy measurements
6. Future improvements
7. Conclusion

1 Introduction

The following document is intended to document the set up and measurements performed during the phase coding demonstration experiments. Following this document an expert laser operator should be able to reproduce and hopefully improve on the results documented here. It is not meant to be a complete and reviewed scientific publication.

One of the main challenges on CTF3 is multiplying the electron bunch rate from 1.5 GHz to 12 GHz. This is carried out using a delay loop and a combiner ring, with high frequency transverse deflectors to separate and combine the electron bunches. For this to work the initial electron bunch train must be 'phase coded' i.e. some of the bunches must be delayed by half of a 1.5 GHz period with respect to the others [1]. With the current thermionic gun this is achieved by subharmonic bunching, which is done over 8 consecutive pulses and causes considerable amount of unwanted satellites in the system [2]. With the laser based photo-injector the phase-coding can be done on the laser pulses before they are sent to the photocathode. The time structure produced by the laser directly correlates with the electron bunch produced.

The source of the laser pulses is a 1.5 GHz mode-locked ps laser (see Table 1.1) The required coding system will delay (or not) so-called "even" and "odd" trains of laser micro pulses which subsequently will result in phase coded sub pulses of electron bunches in the accelerator. The coding does not need to be continuous. It will be sufficient to apply the coding over periods of 140 μ s at up to 50 Hz repetition rate to match the amplification window of the amplifier chain. Each sub pulse will contain 212 laser pulses. The delay applied to the even sub pulses has to be equivalent to a 180 deg phase shift at 1.5 GHz i.e. 333 ps. (See Table 1.2 and Figure 1.1). The specifications for the phase-coding are summarized in Table. 1.2.

The important performance parameters of the coding system include:

Switching time: The system must completely switch from one sub-pulse delay to the next between two consecutive 1.5 GHz oscillator pulses i.e. within 666 ps. Together with the jitter of the switching electronics a rise time of <200 ps on the optical modulator or switch is required.

Stability: There are very tight requirements on the pulse-to-pulse energy stability and the timing stability from the overall laser system. The coding system must not increase the timing jitter of the laser pulses by more than 0.2 ps rms. Variations in the pulse energy must be minimized and ideally they should be kept below 0.1% rms, although higher values than this may be acceptable as the laser system will include both passive and active amplitude stabilization.

Losses: The coding system will be inserted between the existing oscillator and preamplifier. Losses in the coding system will have to be compensated for in the preamplifier and subsequent power amplifiers. These losses should therefore be minimized.

Reliability: The laser system, including the coding system needs to operate for long periods (days/weeks) with very high reliability.

Laser input parameters:

| | |
|--|------------|
| Wavelength | 1047 nm |
| Maximum average power | 320 mW |
| Pulse length (Gaussian FWHM) | 6 ps |
| Pulse repetition rate (cw mode-locked) | 1.5 GHz |
| Time between pulses | ~666 ps |
| Polarisation | Horizontal |

Table 1.1. Laser parameters at the input of the phase-coding

The coding required:

| | |
|------------------------------------|-------------------------------|
| Switching duration | 140 μ s (at up to 50 Hz) |
| Length of sub-pulse | ~140.5 ns (212 pulses) |
| Switching frequency | ~7.1 MHz |
| Delay between generated sub-pulses | 333 ps |
| Pulse timing stability | <0.2 ps |
| Amplitude stability | <0.1% rms |
| Total system loss | <9.6 dB |
| Number of subtrains to injector | 8 |
| Amplitude flatness rms | <0.1% |
| Time delay accuracy | <1ps |

Table 1.2

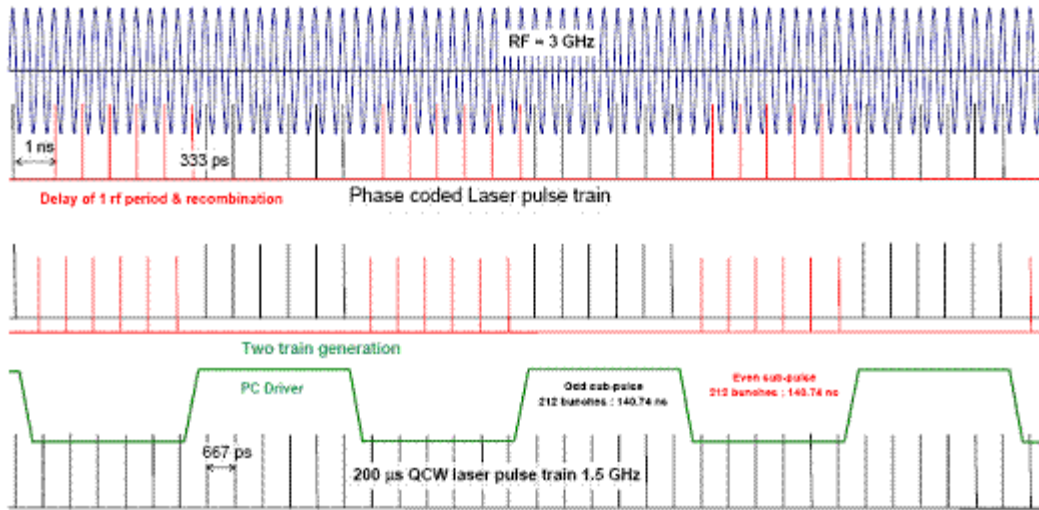


Fig. 1.1 Time structure requirement

2 Design choice

2.1 Pockels-cell option at high power

In the past systems based on fast switching Pockels-cells at the end of the laser chain were considered [3] Fig 2.1.1. However for good transmission at high laser power levels, these cells require large apertures to avoid optical damage, a ~7kV of pulsed drive voltage, together with the fast rise and fall-times <500ps. This places a high average power demand on the driver due to the 50% duty cycle operation for the phase-coding switch and is too challenging for the currently existing solid-state voltage drivers. In addition the relatively long switching time would cause birefringence to build up in the crystal, which is against the EO effect and would cause instabilities or degradation to the flatness of the pulse. The fast switching might also introduce ripples on the top of the pulse train. Further advances in MOSFET drivers and small aperture/low voltage Pockels-cells used directly after the laser oscillator could provide a solution in the future.

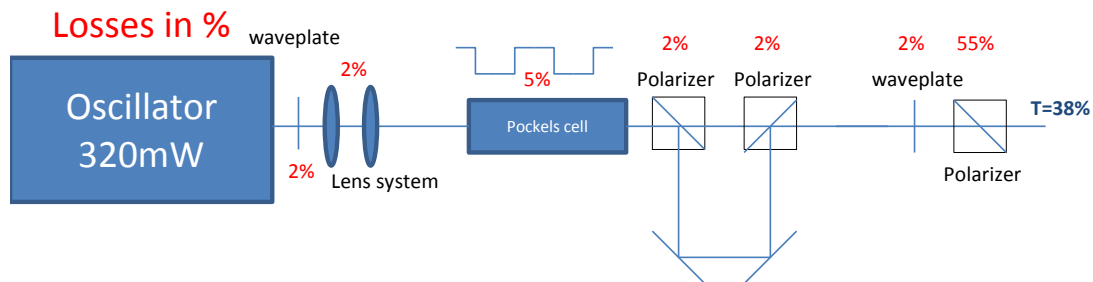


Fig.2.1.1 Possible Pockels cell based phase-coding setup in the infrared

2.2 Fiber optic polarization switch

Electro-optic polarization modulators based on polarization switching dependent on applied voltage could provide a similar solution to Pockels-cell based systems, but with much smaller driving voltages. For example the Versawave 40 Gb/s Electro-Optic Polarization Modulator is capable of changing the state of

polarization (SOP) of light at ultra-high speeds. Functioning as a high speed, electrically variable wave plate, the modulator is able to change the SOP of linearly polarized laser light to an orthogonal linear polarization, passing through elliptical and circular polarization states in between [4]. The range and degree of the change in the SOP can be varied by adjusting the magnitude of the DC bias and RF drive voltage. A possible setup is shown on Fig.2.2.1.

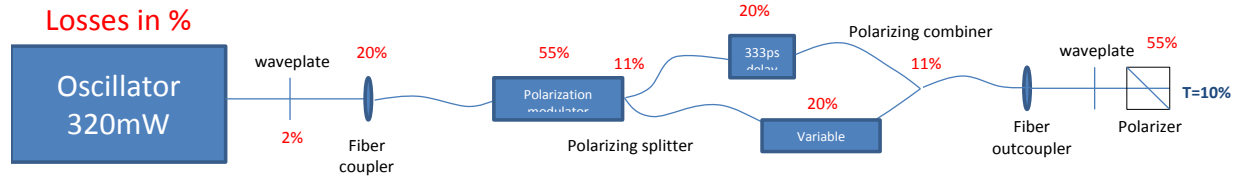


Fig.2.2.1. : Phase-coding system based on fiber optic polarization switches

Because of the insertion loss of the device even two modulators with the second one switching the polarization back after recombination would not help. With this scheme we would have ~30 mW output. As the modulator is made using GaAs, the optical wavelength is currently limited to a wavelength range from 1520 nm to 1570 nm. With some redesign it may be possible to develop a device to work at 1310 nm but operation at 1047 nm is not possible without further R&D on suitable materials.

2.3 Fiber modulator solution

Lithium Niobate (LiNbO₃) fiber optic modulators have been developed at 1 μ m wavelength for amplitude modulation and offer high extinction ratio of 40dB [5]. The waveguide based Mach-Zehnder interferometer consists of a Y split, where the polarized optical input signal is split into two equal components, Fig 2.3.1. One arm contains the electro-optic crystal (LiNbO₃), where phase-shift can be introduced by applying voltage across the crystal. The two arms are then recombined and depending on their relative phase either interfere constructively or destructively, giving an output signal, which is \sin^2 dependent on the applied voltage [6]. The high bandwidth of 10GHz available at the lasers 1047nm wavelength provides the fast risetime necessary for the application. In order to adjust the operating point of Mach-Zehnder modulators independently from the high frequency modulation signal applied, they can be designed with two sets of electrodes: one set of electrodes, the RF Electrodes, is used to apply the RF signal. The second set of electrodes, the DC Bias Electrodes, is generally used to adjust with a fixed voltage the working point of the modulator.

The required system above was called to tender and Photline Technologies was offering the most promising solution, with the following notes [7]:

Laser wavelength 1047 nm: Photline Technologies commercially introduced a range of modulators specially designed to operate in the 1000 nm wavelength region in 2003. The so called NIR-LN family includes intensity and phase modulators that operate in the 980 nm to 1100 nm window.

Polarization: electro-optic modulators are single polarization devices. The reason is the electro-optic effect only appears in the electric field direction. Consequently, one should use a linearly polarized source, possibly terminated with a preserving polarization fibre.

Maximum average power: The NIR-LN modulators have been characterized with an input of up to 100 mW (continuous optical power). Operations at higher power have been experimented but the devices have not been tested for reliability at such levels. 320 mW is above the 100 mW CW recommended maximum optical input power.

Secondly, all performed tests have been conducted with continuous input optical power. For the phase-coding pulsed application Photline has no data in quasi-continuous conditions. Later discussions with a Photline engineer in 2010 suggested, that 4W peak power is the maximum allowed input for pulsed operation in the ps range.

Drifts and stabilization : Lithium Niobate is subject to the photo-refractive effect. That effect increases when the optical wavelength is decreasing and it is noticeable at 1060 nm above a few tens of mW of input power. It translates into drift of the operating point of the modulator and consequently in variations of the output optical power. To compensate for the drift of the operating point, several feed-back loops techniques can be implemented. Photline proposed the MBC-1000 Modulation Bias Controller that locks the operating point of the modulator at a user selected position. The principle relies on applying a low frequency tone signal to the DC electrodes of the modulator and analyzing the modulated optical output power. The frequency and amplitude of this modulation has to be set right for the operating point (QUAD+/-) and will depend on the time-structure of the produced signals. The Photline engineer also suggested temperature stabilization to 40deg, which has produced good results at the factory. In addition special attention must be given to the driving electronics to reach the required power stability of the resulting optical signal.

Length of sub-pulses : 140.5 ns. This is compatible with the rise and fall time of the proposed modulator as long it is correctly driven. Special attention must be given to the drive electronics to optimize the rise and fall time of the resulting optical signal. An AC coupled driver DR-PL-10-MO-LR was purchased from Photline in 2010 to achieve flat pulses over the required period with adjustable gain.

Pulse timing stability : 0.2 ps. The modulator is not known to bring additional jitter to an electronic driving signal. However special attention must be given to the drive electronics to reach the high required timing stability of the resulting optical signal. An additional point here is, that as the driving voltage only provides the window for the pulse-train it does not inherently affect the jitter of the individual pulses, as long as the rise-time is well below the 666ps separation of the pulses.

2.3.1 Initial tests/ one modulator scheme

The original setup implemented at STFC CLF [8] and later further studied by INFN [9] is shown on Fig.2.3.3.

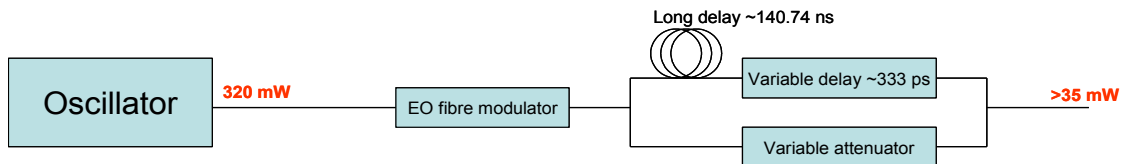
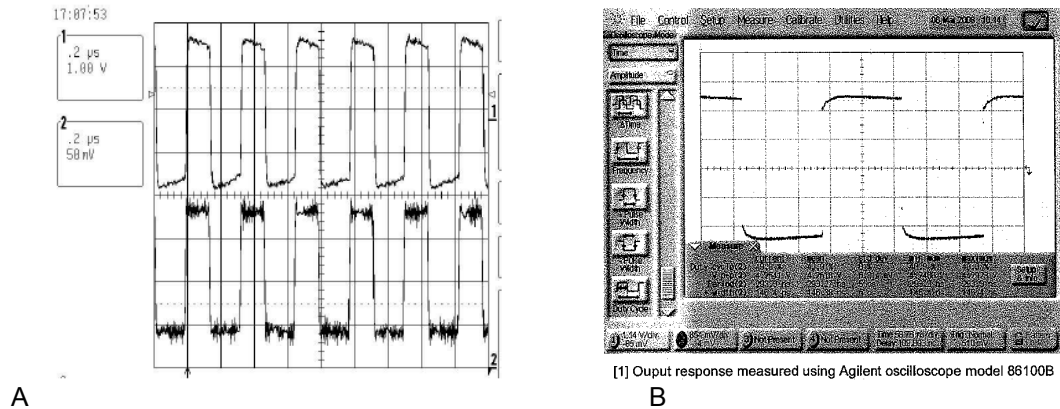


Fig.2.3.1 Single modulator setup

These studies have revealed several problems:

- Instabilities were observed from the modulator and bias control mainly due to high input powers of 160mW. This power was above the safe 100mW limit specified by Photline to avoid losses and heat dissipation related instabilities. As the bias controller is using the signal from a photo-diode placed by inside the modulator housing to feed back on the drive voltage, heat effects will cause incorrect bias settings.
- Flatness of the used DR-GA-10 driver was not satisfactory (Fig.2.3.2). Later discussions with Photline suggested that the incorrect impedance matching to the driver input could have caused profiles measured in (a), however sloping risetimes measured during delivery test were unavoidable.



*Fig.2.3.2. Output response of the DR-GA-10 driver amplifier with flat input voltage
a) measured at INFN using input from pulse generator (bottom curve shows input pulse and top shows output response)
b) test report by Photline upon delivery*

- Fibre launch system was not accurate enough to achieve good coupling efficiencies into the fiber and required regular realignment.
- Fibre core sizes were not matched and connectors were not compatible, some with European and some with US standard sizes.

The overall performance for transmission is shown in Fig. 2.3.3.

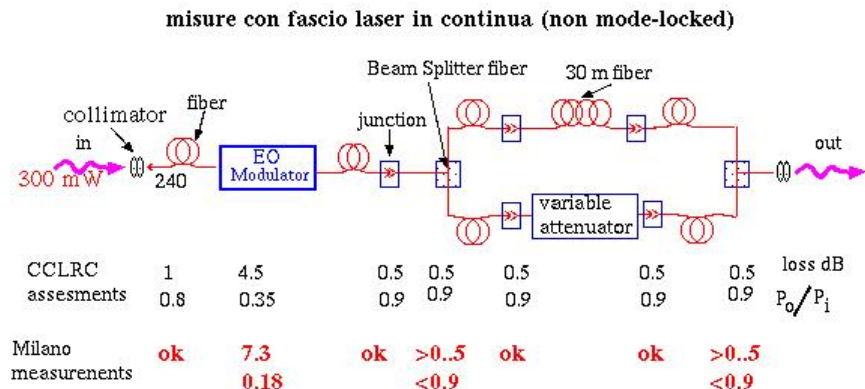


Fig.2.3.3. Transmission measured at RAL and at INFN

- INFN reported a decrease of output from the modulator over time (18% to 7%). There was also earlier data from RAL, which shows 36% transmission. The modulator was sent back to Photline and the input fiber was found to have been damaged due to high input power levels.
- It was apparent, that without further amplification the system would not provide enough power throughputs.
- Furthermore a 140.7 ns fiber delay line is necessary with less than 500fs timing accuracy. Resistors were installed to heat the plate holding the fibre bundle, but no power supply and monitoring device for the temperature stabilization was implemented. After accurate cutting of the fibre, temperature can be used for fine alignment and has to be kept at $\sim 0.2^{\circ}\text{C}$ accuracy to achieve the required timing stability. From the temperature induced refractive index variation $1.92\text{ps}/^{\circ}\text{C}$ can be calculated for the 30m delay fibre.
- The fibre used (Cicorel UK, polarization maintaining singlemode fibre patchcord FC/PC to FC/PC on jacketed fibercore HB980T) was optimized for shorter wavelength. In INFN they reported 15%

loss in the fibre and 10% loss at each connection. Variable attenuator was not implemented on the system.

2.3.2 Two modulator scheme

In light of the previous test several improvements were made to the system. The design was changed to a two modulator scheme shown in Fig. 2.3.2.1. The main modifications are listed below:

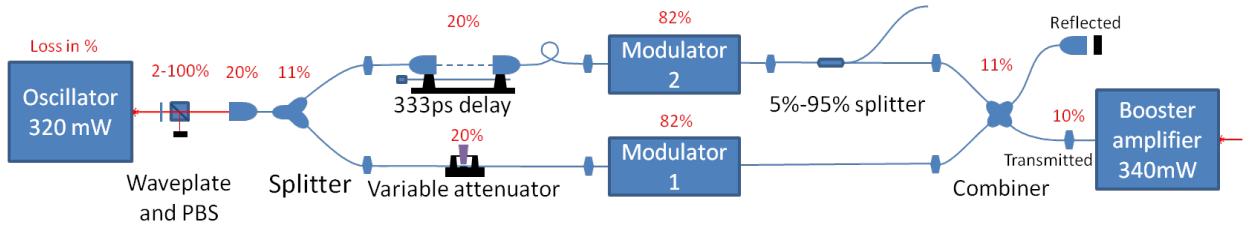


Fig.2.3.2.1. Two-modulator based scheme with measured losses

- Two-modulator scheme is safer against power damage. Lossy elements, such as the fiber splitter, attenuator and the delay line can be placed before the modulators. Furthermore the power is split in between the two modulators. This way full power of the 320mW oscillator can be utilized without the risk of exceeding the safe 100mW power limit for the modulators.
- As the total delay introduced is only 333ps between the two arms, sensitivity to temperature changes is very small, well below the requirement.
- A fibre oscillator purchased from Fianium provides amplification back to the oscillator power level of 320mW and includes an active feedback stabilization system with $\sim 100\mu\text{s}$ response time to ensure constant output power by adjusting the pump current. The amplitude stability measurement was carried out by monitoring the mean value over the 500 microsecond 'amplification window' for the laser chain and over 215 shots using Thorlabs DET10A. Fig 2.3.2.2

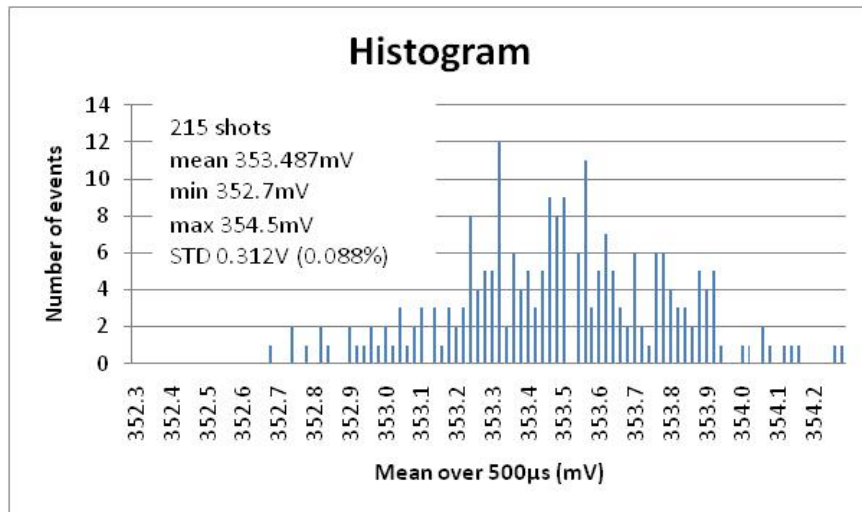


Fig. 2.3.2.2: Stability measurement of the laser booster amplifier

- The required RF modulating signal to drive the modulators was produced by a custom made circuit designed at CERN (Stephen Livesley, A. Andersson). A low phase noise 1.5GHz beam synchronized signal was provided and capacitively coupled to an 8 bit programmable ECL counter (MC100EP016F). The counter was followed by a D flip flop (MC100EP31DG). These circuits together allow the selection of a pulse length within the required range (140ns) and the terminal count output connected to the D flip flop creates the required square wave signal. The

signal is only delivered for the amplification window of the burst mode amplifiers (AMP1, AMP2) to allow resynchronization between each burst. The electronics box also includes AC amplifiers (DR-PL-10-MO-LR) which provide the fast rise times necessary and will also dampen variations on the driving voltage. With the 300ps accuracy of the switching, cutting between two consecutive pulses can be easily ensured by choosing the right cable length between the output of the driver box and the modulators. Fast trigger signals to start and stop the counters, also synchronized to the RF frequency, were provided by CNT6 and CNT7.

- Driver amplifier with improved square pulse response was purchased to improve flatness of the sub-trains. As within the 666ps cycle time the pulses are 5.5 ps long, both the in house switching system and the driver amplifier provide the flatness in the 140ns switching period.

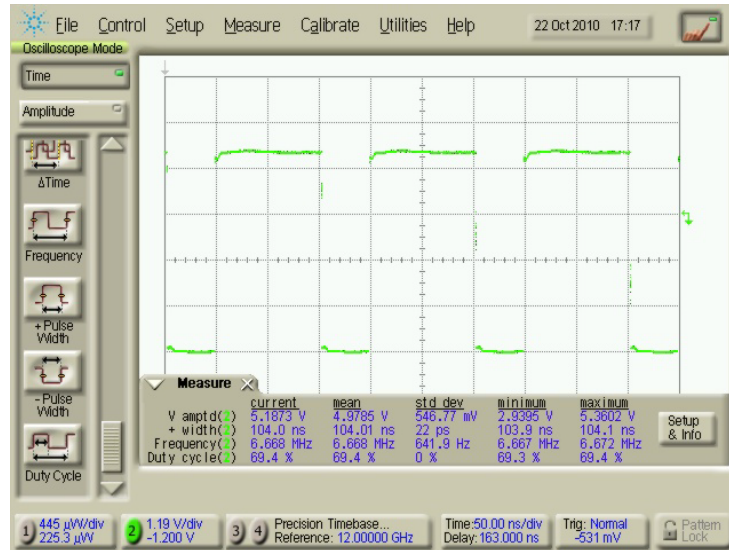


Fig. 2.1.2.2. DR-PL-10 test performed at Photline

3 System setup

3.1 Online amplitude- and phase-adjustment

A diagnostic was needed to provide easy, accurate and preferably online measurement of the timing difference and the amplitude balance between sub-trains.

Photo-diodes provide fast and accurate measurement for both timing and amplitude. Our highest bandwidth photodiodes are fiber-coupled the New Focus 1024 with an impulse response of 12ps FWHM, and the New Focus 1014 with a 3dB bandwidth of 45GHz. The New focus 1024 is optimized for time domain measurements and the 1014 is optimized for frequency domain measurements, however they were both found to be well suited for both applications in this case, although the 5.5ps laser pulses cannot be fully resolved by these detectors.

While the delay can be roughly set using the digital oscilloscope LeCroy Serial Data Analyzer SDA18000 (18GHz, 60 Gsamples/s), this does not provide an accurate measurement, because of the timing jitter of the trigger signal and the digitization itself. Furthermore the oscilloscope cannot be triggered on a balanced train as the sub-trains are not distinguishable, so a single trace has to be recorded and post-processed, which can be very tedious. Post analysis provides accurate evaluation of the timing switch, but not a fast setup with visual aid.

It is possible to check the output signal in the frequency domain. The Fourier transform of a train of Gaussian pulses, consists of spectral lines at multiples of 1.5GHz and of course at DC. If a part of this signal is phase shifted, other frequency components also appear, depending on the sub train length.

3.1.1 The frequency domain method

When no drive voltage is applied to the modulators a continuous 3GHz signal will be created after recombination of the two 1.5 GHz arms with half of the nominal amplitude due to the QUAD (50%) working point of the modulators. Detailed explanation on the mathematics of the signal evolution at different multiples of the 1.5 GHz can be found in ref. 10. As we approach 180° phase shift odd multiples of the 1.5GHz the lines will disappear from the spectrum while the even multiples of the 1.5GHz the spectral lines will corresponding to a clean 3GHz periodic signal spectrum increase. At different amplitudes of the two signals however the odd spectral lines will remain with some non-zero amplitude even at perfect time-delay.

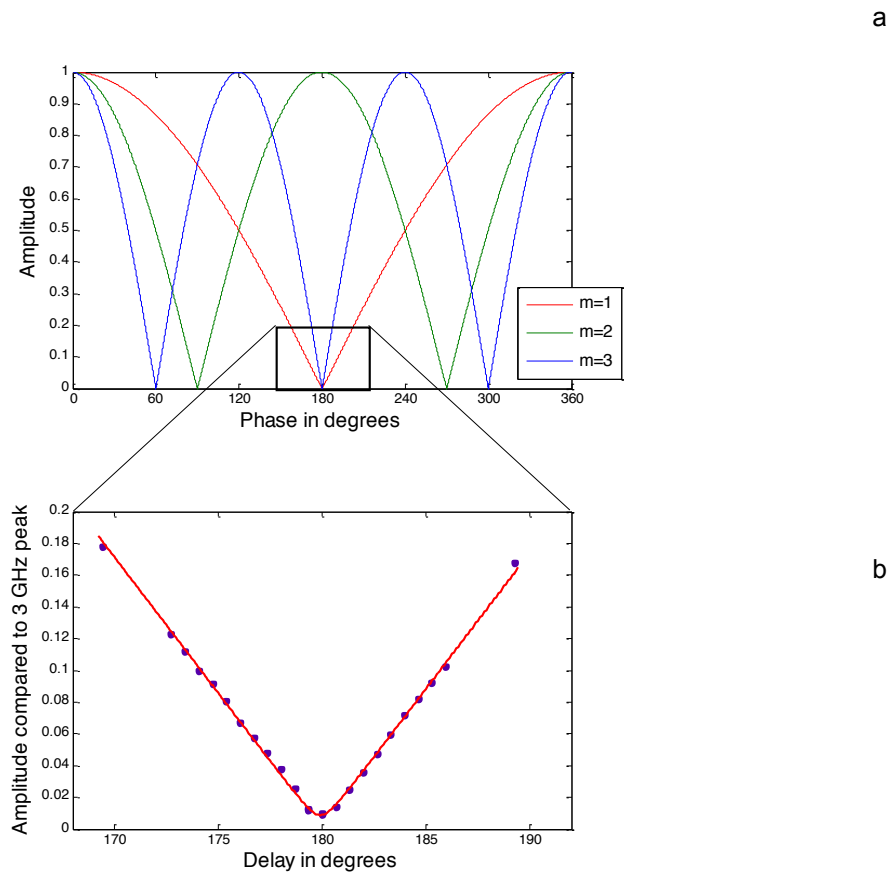


Fig.3.1.1.1 a) Expected variation of the spectral line relative to the peak at different frequencies with perfect amplitude balance; b) Amplitude of the 4.5GHz peak respect to the 3GHz main peak with fit including amplitude error

By minimizing the 4.5GHz peak through iteration of time and amplitude adjustment, peak suppression 40-67 dB below the 3 GHz reference was achieved depending on the noise arriving from the oscillator noise on each day. This corresponds to a maximum amplitude error of 1.76-0.044% with maximum timing error of 0.1-0.016 ps. The change of the 4.5 GHz peak by varying delay is shown on Fig.3.1.1.1 The effect of

time delay on the spectrum is greater if we look at higher multiples of 1.5 GHz, unlike the effect of the amplitude imbalance between the arms. Measured accuracy was limited by the finest adjustment possible manually in the delay and attenuator arm and shows that with stable input source phase-coding scheme can provide accurate settings well within specification.

Changing the amplitude of the delayed sub pulse train pulse, changes the size of the spectral lines at 1.5GHz or any of its multiples in the same way: the amplitude increases linearly with the imbalance regardless of which arm is more intense. The effect of time delay on the spectrum is greater if we look at higher multiples of 1.5GHz, unlike the effect of the amplitude imbalance between the arms.

The frequency domain method is capable of setting the delay and amplitude balance to accuracy significantly better than 0.1 ps and 0.1%. The great accuracy can be achieved due to the high dynamic range of the spectrum analyzer. A great advantage of this measurement method is that noise, such as detector noise, generally increases the measured peak and thus makes our calculations of maximum amplitude balance and delay error conservative. The fluctuation is greater when the amplitude of the peak measured at harmonics of 1.5GHz is smaller. This partly due to the nonlinearity of the decibel scale, and partly due to the fact that the fluctuation in one arm becomes more significant compared to the peaks average value as the peak gets smaller (the peak linearly increases with amplitude balance error if the timing error is small).

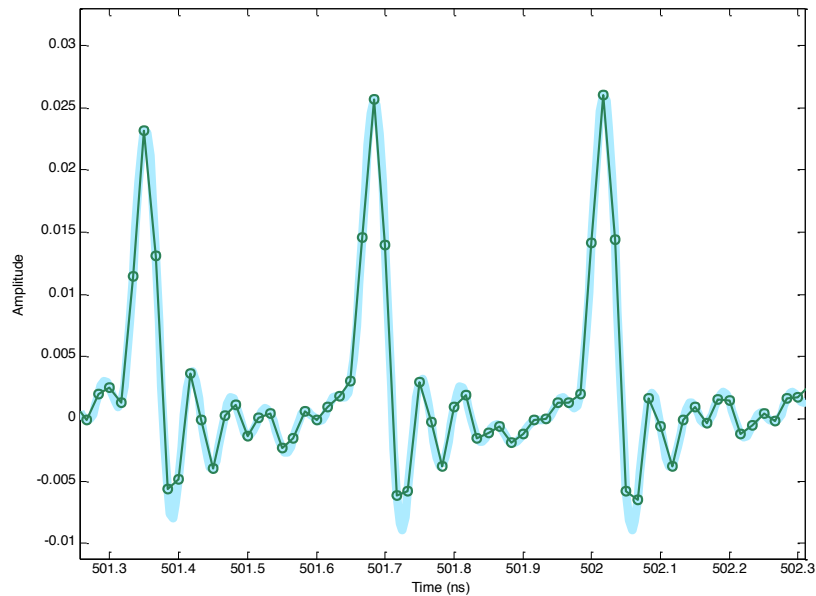
The limiting factors are:

- Fluctuation of the measured peak due to noise for, the laser oscillator, which limits the accuracy
- Modulators have to be off, this can cause drifts of the working point and so for amplitude error measurement between the arms time domain method is preferred.

The drift of the in fibre attenuator was a major problem. As the measured peak has drifted accuracy for setting the timing goes down. This was solved by replacing it with a variable neutral density attenuator wheel.

3.1.2 The time domain method

As previously mentioned the delay can also be measured by oscilloscope, the best oscilloscope available in the lab was the LeCroy Serial Data Analyzer SDA18000. This oscilloscope has a bandwidth of 18 GHz, and New Focus 1024 photodiode an impulse response of 12ps FWHM.



3.1.2.1. Figure. An oscilloscope trace and four times $\sin(x)/x$ interpolation

This results in our 5.5ps pulse appearing as a roughly 35ps wide pulse (FWHM), with some post-oscillations. With the 60 Gsamples/s rate a point is taken every 16.7 ps. This means that 4-5 points are recorded during one pulse. The interval accuracy is 3.3ps. (The trigger jitter is specified to be 2.5ps RMS.) As mentioned earlier the jitter of the laser is about 0.5 ps RMS to the reference of 1.5GHz. This means, that the delay cannot be directly measured accurately between two consecutive pulses at the switching. This can be solved by saving a trace and post processing using the following algorithm: The time of each pulse is recorded; a phase for each pulse is calculated using the oscilloscopes internal clock as reference. The average phase of the pulses from the attenuator arm is then subtracted from the average phase of the pulses from the delay arm. With a large number of pulses the phase jitter of the laser and the phase jitter of the sampling will decrease proportional to \sqrt{n} , where n is the number of samples. Another advantage is that the method can be used when the modulators are on.

A $\sin(x)/x$ interleaving is applied directly on the oscilloscope. The trace is copied from the oscilloscope and processed on a PC with MATLAB. A trigger level is set. The first sample point above this level and the previous point are used, with a linear fit, to determine the time when the signal crosses the trigger level, Fig 3.1.2.2. From this time the pulses expected time, according to the oscilloscopes time base, is subtracted. The expected time of a pulse in this sense is the number of pulses so far times the nominal time between two pulses. The result of the subtraction is phase of the pulse. It is important to note that this is implemented in a way to avoid underflow even with a large number of pulses.

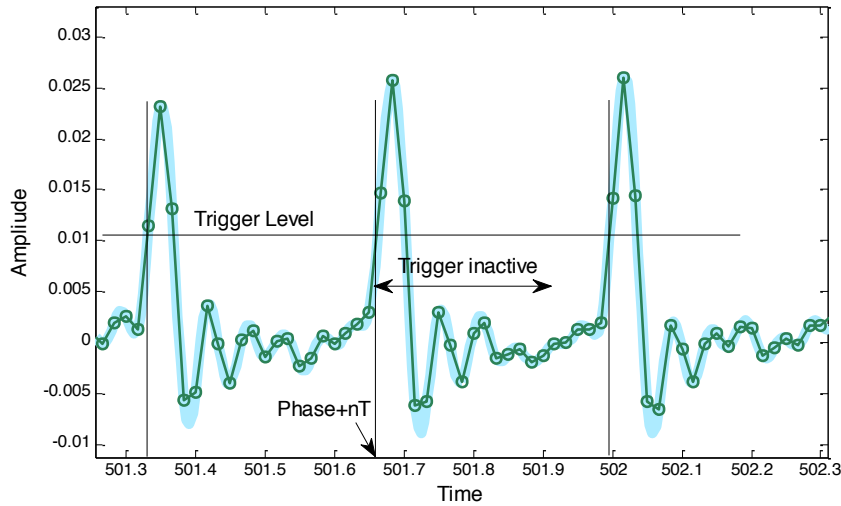


Fig.3.1.2.2. Trigger definition for post processing

Because the pulse repetition rate is not exactly 1.5 GHz and because the oscilloscope time base is not perfect, the measured phase is constantly drifting in one direction. This can be corrected by applying a linear fit to the phase and then subtracting values of the fitted curve. The resulting corrected phases for the pulses from the delay arm and the pulses from the attenuator arm both follow more or less Gaussian distributions. The difference between the mean of these phases gives us the delay + delay error. When the method is used with the modulation on it is important to use an equal and integer number of odd and even sub trains, as input.

3.1.3 Comparison of accuracy between the two methods

The 10.5 GHz peak was used for the spectrum analyzer measurements to demonstrate the increased delay sensitivity. In initial setup the 10.5 GHz peak was 44.1 dB below the 9 GHz reference. This corresponds to a maximum of 0.6% amplitude error or a maximum delay error of about 0.19 ps.

These measurements (seen on 3.1.3.1) were done with 4 times interpolation and calculated from almost 300,000 pulses for each point.

| | Delay error | Amplitude error |
|------------------|-------------|-----------------|
| 1 trigger level | -0.027 ps | 1.31% |
| 2 trigger levels | -0.136 ps | 1.31% |

Table 3.1.3.1

From the delay error and the amplitude error determined in the time domain the expected magnitude of the 10.5 GHz peak can be calculated.

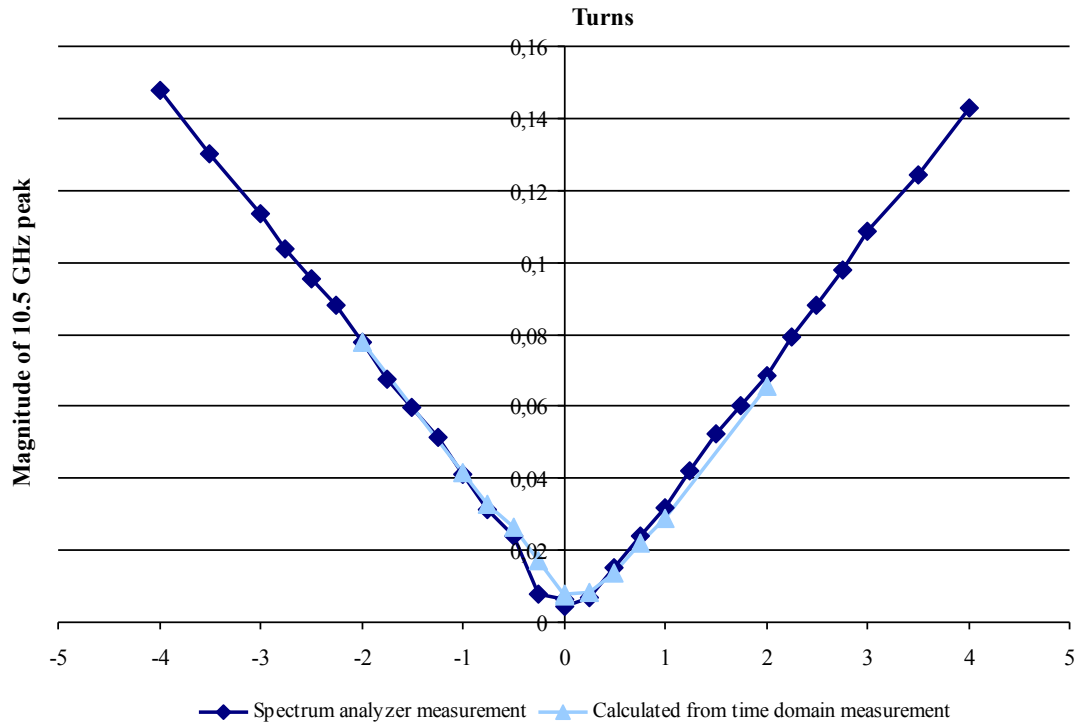


Fig. 3.1.3.2. Comparison of time delay with the two methods

As seen on Fig 3.1.3.2 the calculated and measured values fit each other very well. From this we can conclude that amplitude error measured in the time domain is larger than in reality. As mentioned before the accuracy of the amplitude error measurement can be greatly improved by applying this method to the phase-coded train.

3.2 Components

3.2.1 Coupling into the fibre

In order to couple light into an ω diameter fibre with a D ($1/e^2$) diameter beam the ideal focal length is

$$f = \frac{D}{\pi\omega}$$

, where λ is the wavelength. In our case the fibre is $\omega=6\mu\text{m}$ and the oscillator output at this point is 2.2mm, which suggests an optimum focal length of 11mm. New objectives were purchased to improve coupling efficiency, but as they arrived after the experiment, they have not been tested for improved coupling efficiency.

3.2.2 The 50/50 splitter/ combiner from Photline

Due to either connector/fibre incompatibility the output measured though arm 1 was 25.4% and through arm 2: 24.5%, this is for the splitter SN: 7317. In the case of splitter SN: 7504 arm 1 only had 7.5% transmission. These splitters can also be used for the combination of the two beams to ensure the same polarization from the two arms, although the overall transmission cannot exceed 50%. Polarization based combiners have been purchased from Ozoptics with high transmission, but the two combined arms carried opposite polarizations, where only one arm was amplified by the booster amplifier. This is due to

the fact, that a Faraday isolator is placed inside the booster amplifier. Although booster amplifier could amplify both polarizations the Nd: YLF amplifiers could only amplify one due to the birefringence of YLF.

3.2.3 Modulators

Care should be taken not to have more than 100mW average and 4W peak power input into the modulators. By scanning the bias voltage either manually or automatically one can find the maximum transmission operational point. Here we have measured a transmission of 24.3% for modulator 1 and 27.4% for modulator 2, including losses on the connections. One should note that both halfwave-voltage and operating point bias are drifting with temperature. Photline suggested temperature stabilization to 40°C as the active bias control is not optimized for our 50% duty cycle transmitted signal case. Settings can vary from day to day depending on the laboratory conditions.

3.2.4 Delay line

The Ozoptics 35856 ODL-100-11-1053-6/125-P-40-3A3A-1-0.5 variable delay is based on a manual translation stage between two collimator lenses and is a free space device, which must be used in a clean environment. The total length of the stage only allows 300 ps delay and so additional large delay to one arm might be necessary to get into the required 333ps delay range. In our case a 95/5 tao purchased from Photline was used to compensate for the mission delay. The 5% output from the delay arm can be also useful for monitoring bias drifts in the future.

3.2.5 Attenuator

The Ozoptics 33686 BB-700-11-1053-6/125-P-50-3A3A-1-1-LL variable attenuator is based on a small screw interrupting the beam between two collimator lenses. Although we have not exceeded the average power specification it is possible that backreflections from the screw can cause damage to the collimators with a pulsed laser. Over time we have observed decreasing throughput with the screw removed from the beam. Waveplate and polarizer based attenuators with remote options exist from Ozoptics and would provide a more robust solution for the future, also with the possibility to use it as part of an amplitude feedback.

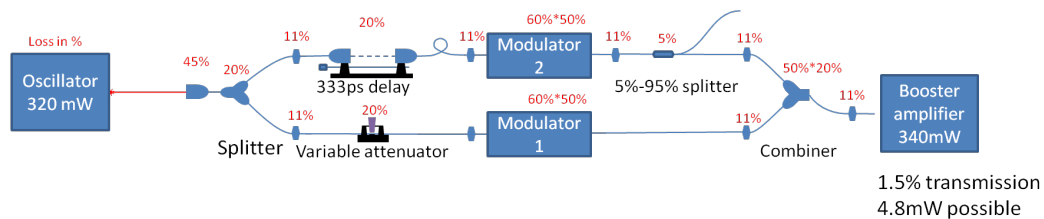


Fig. 3.2.2.1: Total losses in the system

3.3 Assembly

3.3.1 Fiber input set up to the Thorlabs Nanomax stage:

- Set input power to maximum 1W (in case of oscillator max. 320mW available.)
- If oscillator is used install Faraday isolator between nanomax stage and fiber input as disturbed mode-locking was observed due to backreflections.
- Make sure light is entering the stage at normal incidence both horizontally and vertically (a pair of input mirrors are the best suited for this purpose)
- Check with card, that light exiting through the fibre mount is centred on the pinhole
- Install yellow Thorlabs single mode fibre for initial setup onto Nanomax stage

- Put other end of the fibre in front of the CCD camera
- Optimize the throughput with camera, first by optimizing objective position and then iterating with X,Y,Z of the fibre mount.
- Once light intensity is high, continue the optimization with a power meter in place of the camera.
- Expected transmission/coupling is ~50%
- Exchange fibre to Thorlabs blue single mode/ polarization maintaining one and reoptimize with X,Y and Z using the power meter. As the modesize is smaller then 40% is the typical value achieved here.
- Install fibre splitter from Photline and check transmission. A total transmission of ~50% is expected from the two arms together.

3.3.2 Delay setup

- First assemble the system without the modulators to get familiar with the delay setup.
- Install variable fibre attenuator on the arm1 of the fibre splitter and the manual delay line on the arm2 of the fibre splitter.
- Use Ozoptics splitter/combiner (32775 FUSED-12-1053-6/125-50/50-3A3A3A-1-1-PM) to recombine the signals.
- Connect the output signal to SDX18000 LeCroy scope for timing delay analysis.

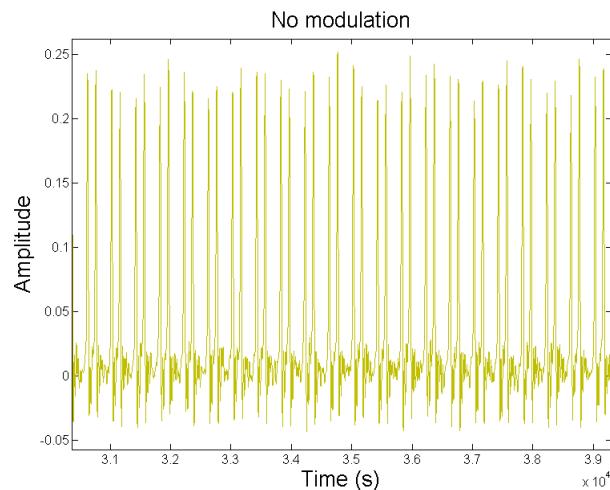


Fig. 3.2.2.1 Delay error between the two arms

- The amplitude balance is restored by adjusting the fibre optic attenuator (later this was left at fixed position as damage was observed after repeated changes and was later replaced by a variable attenuator in the free space delay line.)

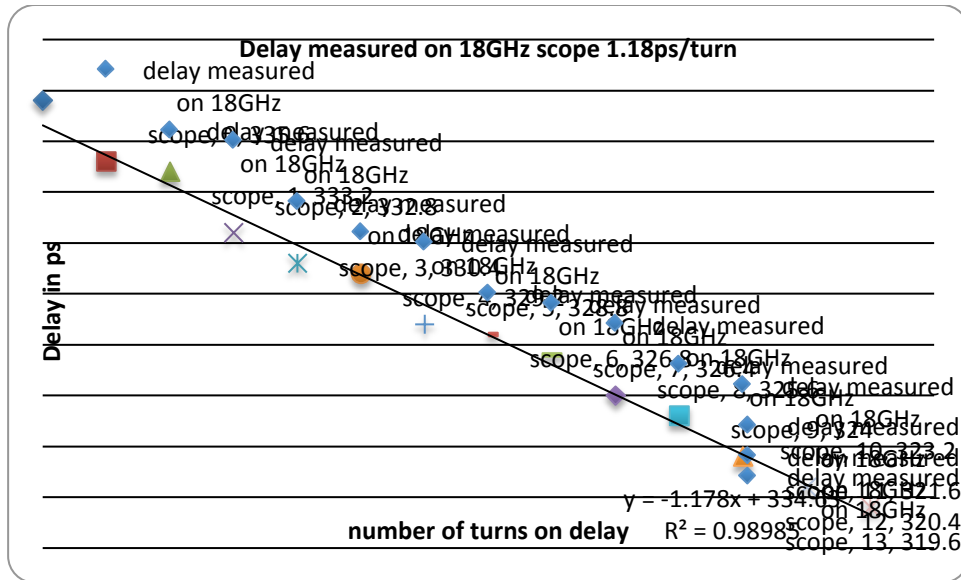


Fig. 3.2.2.2. Delay calibration with oscilloscope

- Once delay is set for equal time between the two trains on the oscilloscope by turning the delay line, connect signal to the spectrum analyser, Fig 3.2.2.1.
- Observe the peak at 4.5 GHz.
- The fibre optic attenuator is adjusted until the peak is minimized.
- Then the time delay is adjusted to decrease the peak at 4.5 GHz, Fig 3.2.2.2.
- The two steps are repeated until noise floor is reached.

3.3.3 Modulator transmission setup:

- Add modulators after the attenuator and delay line. Make sure; that the input power at the input of the fibre stage is no more, than 650mW, to avoid damage to the modulators.
- As the new modulator (MOD1) has better transmission it should be installed in the attenuated arm. The signals are then recombined and observed the same way as above. Each arm is observed independently at the start.
- The basic operation of the modulator and the bias controller can be found in the users' manual. Here only the practical tips are mentioned for setting the QUAD working points.
- Bias point drifts with average power load on the modulator.
- For fast setup use the built in scan of the bias controller to find MAX and MIN operating points. Take the mean value of the two for QUAD setting. Alternatively scan with MANUAL option the bias voltage and monitor the fibre output from the modulator on the oscilloscope. A full scan is shown below, Fig 3.3.3.1.

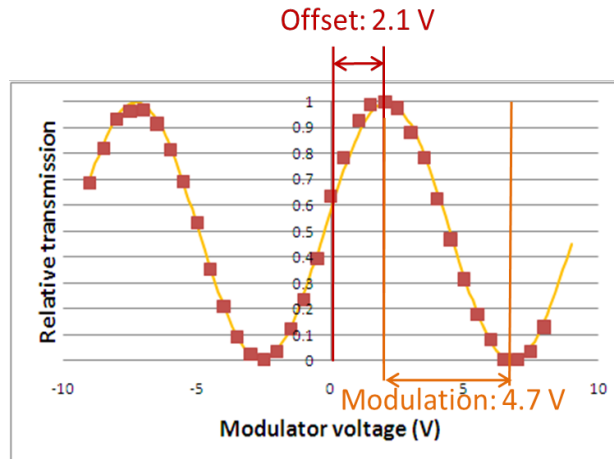


Fig. 3.3.3.1.: Modulator transmission versus bias voltage measurement for setting QUAD operating point.

3.3.4. Driver setup

- Please note that drivers should not run, when they are not correctly terminated, so signals should either be connected to a 50Ω terminated scope or to the modulators.
- As modulator halfwave-voltages are known from the previous measurement the signals can be connected first to an oscilloscope to check the voltage levels are set correctly in the driver amplifier. In our case typical values for V_{π} where 4.93V for Mod1 and 4.87V for Mod2.
- Connect timing signal to the driver box to trigger the switching. One STOP and one START signal is required. Counters normally used for CALIFES pulse pickers were connected for this purpose.
- There is no power switch, so once the cables are connected, plug the device into the mains.
- Observe the signals on the scope and adjust the voltage to the measured level for each driver output. Two potentiometers-crews are on the front of the driver for this purpose.
- Unplug the driver box and connect the signals to the modulators.
- Observer recombined signals on the oscilloscope with driver box on and modulators biased to QUAD+ and QUAD-.
- The timing of the driver switch determines the envelope of the sub-trains. It is necessary to set the cable length from the driver to the modulator to make sure, that switching takes place in between pulses and not cutting through them. Observe the start and end of pulsetrain over several shots as the jitter is ~140ps.

3.3.5. Final adjustment

- Set timing between odd and even sub-trains to 333ps and check 140ns later, that 999ps switch is also present.
- Block the delay arm and check, that there are no background pulses. Adjust QUAD setting. NO adjustment of the drive voltage should be needed!

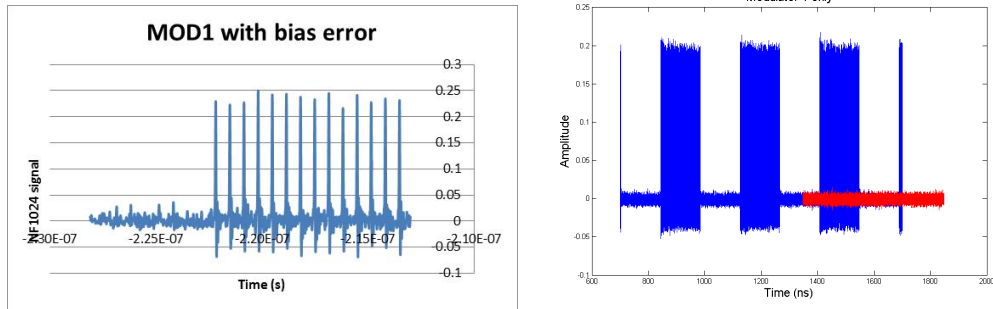


Fig. 3.3.5.1 Bias error on MOD1 manifest is small background pulses in the OFF state (left), which disappear into the noise floor when bias setting is correct (right)

- Disconnect attenuator arm and repeat with the unblocked delay arm.
- With both arms connected set delay and amplitude balance as well as possible between the two arms.
- Switch off driver and leave on bias controllers.
- Connect the signal to the spectrum analyser.
- Optimize, as described in 3.3.2.
- Turn the drivers back on a let the system stabilize for 15 minutes.
- Check again on spectrum analyser and optimize if necessary.
- The system is now ready to be connected to the laser chain.

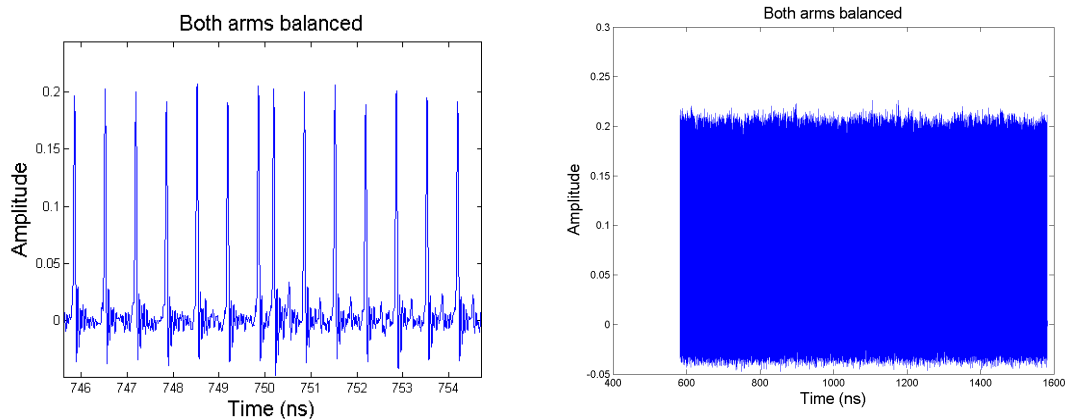


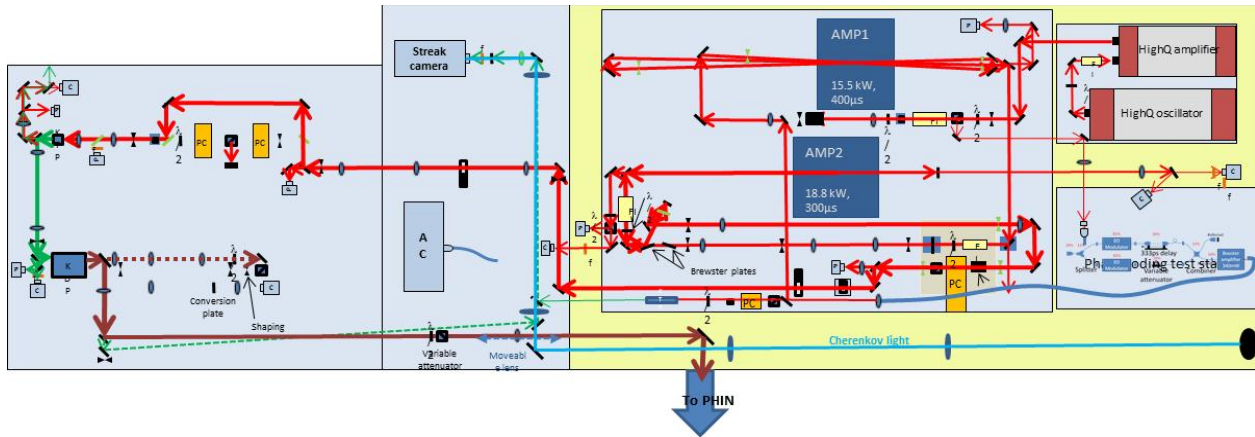
Fig. 3.3.5.2: Typical oscilloscope traces when phase-coding is set up.

4. Integration into the laser chain

Several modifications were necessary to the laser system to accommodate the phase-coding setup, Fig 4.1.

- Interlocks had to be modified to make sure AMP1 and 2 turn off in case of failure to the booster amplifier.
- Output of the booster amplifier had to be matched to the rest of the laser chain both in power and in size.
- Amplification of the phase-coding had to be confirmed at several stages of the system, so additional beam-paths had to be created to send the beam to the streak-camera station.

- As power of the oscillator was not sufficient to drive the phase-coding without?? the booster amplifier, part of the HighQ preamplified beam had to be coupled into the fiber.



Legend:

- | | |
|----------------------------|-----------------|
| Mirror | Periscope |
| Lens | Camera |
| Halfwave plate | Photodiode |
| Faraday isolator (or part) | Shutter |
| Polarized beam splitter | Filter |
| Pockels Cell | Optional iris |
| Power meter | Optional mirror |

Fig. 4.1 Setup of the laser system including optional beam passes for streak measurements.

4.1 Fibre amplifier

The fibre booster amplifier was designed to run with a minimum of 10mW input to ensure that final output power of 320mW is reached with a high level of saturation for stability. There is an interlock built into the system, which turns the amplifier off when the seed is lost to avoid damage due to ASE. This is triggered, when the input signal level drops below 5mW. Due to the low damage threshold level of the fibre modulators and the number of connectors in the system as well as the 75% inherent loss due to the switching and non-polarizing recombination, -as mentioned in paragraph 3.2- the maximum achievable output from the system is <5mW. After discussions with the company the seed error limit was dropped to 4mW and the maximum output power revised down to 250mW. Despite this we have found that the system was repeatedly producing output error, when run at these extreme parameters and lowered the output to 200mW for operation. N.B. the factory password needs to be acquired each time a modification to the system is done.

Amplification with the fibre booster amplifier was measured and switching was confirmed with streak camera measurements and with the freespace fast photodiode (AlphaLas_UPD-40) on the SDA18000 oscilloscope, Fig 4.1.1. Please note, that Pockels-cell was necessary to gate out the cw mode-locked signal from the booster amplifier to make the streak measurement possible.

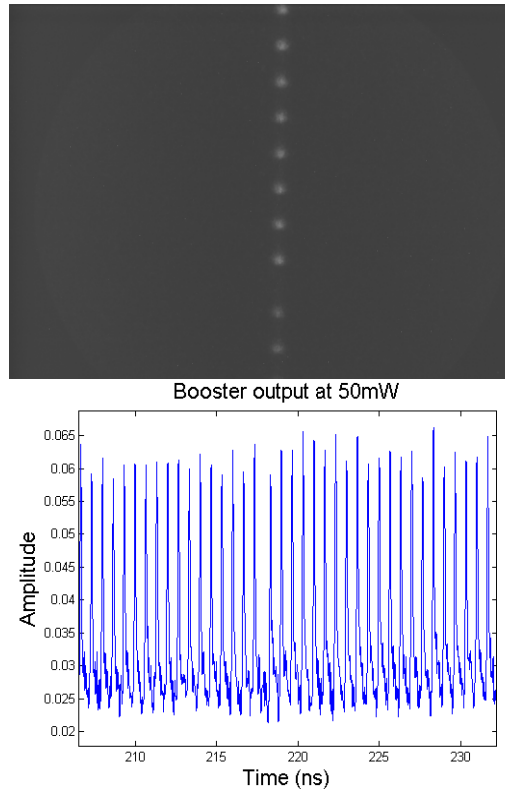


Fig. 4.1.1 Streak camera measurement at second harmonic of the booster output (left) and PD measurement at the fundamental (right) showing the 999ps switching.

4.2 Beam profile and stability

There are many advantages in using the fibre based amplifier to power levels below the threshold where non-linear effects appear and where bandwidth broadening does not make later stages of amplification inefficient. After discussions with Fianium it was concluded, that 10W out power can be delivered at 1047nm wavelength with <1nm spectral bandwidth and < 10ps pulse length. The spectrum is within the gain bandwidth of Nd:YLF and the pulselength after harmonic stages would still provide the specified <10ps pulses on the cathode. However the purchase of the 10W amplifier was not possible at this date. We made the following remarks on the laser:

- Fibre booster amplifier was found to provide exceptionally good beam quality.
- As the delivery is through a fibre, the pointing stability of the front end of the system is determined only by the stability of the optical mounts and not the stability of the laser, such as the solid state HighQ pre-amplifier
- These two together results in less daily alignment of the system
- Amplitude stability is regulated by an internal feedback and was measured at 0.08% RMS
- Currently, with the 200mW input to the amplifiers we reach higher UV at the end of the system due to the improved beam quality (before we had 7.5W from the HighQ preamp as an input)

4.3 Full amplification/ Harmonics

The scheme above was planned, where the oscillator output provides the input for the phase-coding, after the losses are recovered by the recently purchased fibre booster amplifier. The output is then amplified

with HighQ preamplifier and the high power amplifiers as in the original system. HighQ was not willing to do the modification without sending all the parts, including phase-coding and booster amplifier to them, which was not an option given the complexity and the operational constraints. We could do the modification at our own risk. Possible damage to the amplifier crystal would result in 4 weeks delay (we would have to send it to them for repair) and 18000 CHF repair cost.

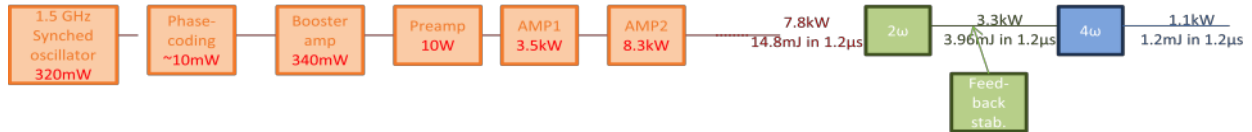


Fig. 4.3.1 Original setup including pre-amplification to 10W

Tests were done on the AMP1&2 stages to find out how much energy per pulse could we expect, if we reduce the input to AMP1 and AMP2 from the usual 7W to 250mW (including losses between the fibre output and the APM1 input.) Close to nominal 350nJ/ pulse was still achievable with these parameters.

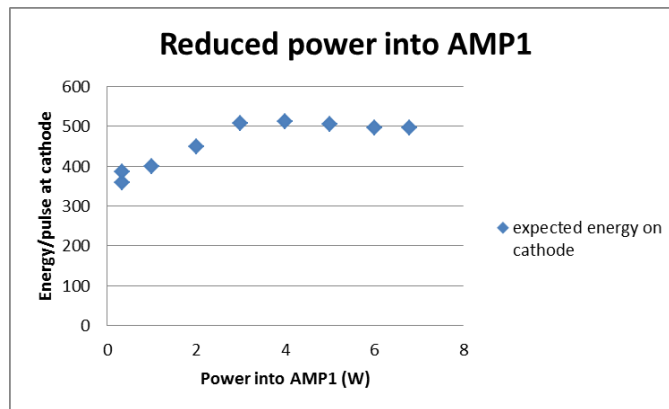


Fig.4.3.2 Expected energy/pulse (nJ) on the cathode with reduced input power to the amplifier chain.

Therefore the following setup was chosen Fig 4.3.3.

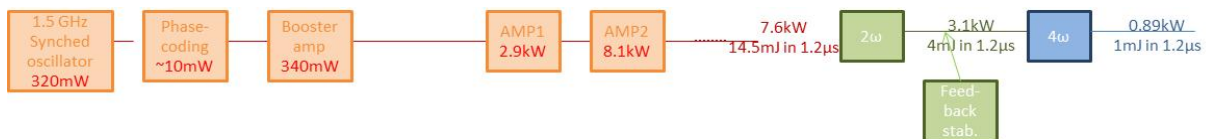


Fig.4.3.3 Amplification scheme chosen for the final setup

Beam size matching of the fibre booster output to the amplifier chain was still necessary. The output of the fibre collimator was measured –with UEye digital USB camera- to obtain the right lens system.

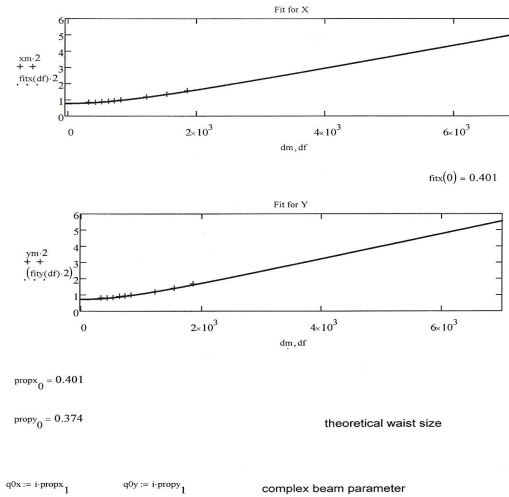
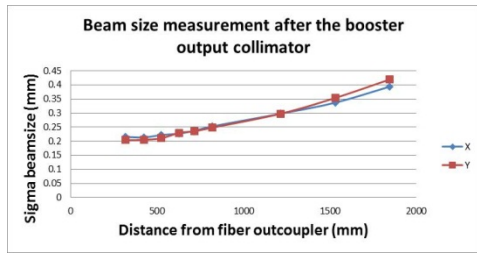


Fig.4.3.4 Beam size as a function of distance from the exit of the fibre booster output-coupler and beam size prediction at the end of the AMP1

By applying Gaussian beam propagation fit here, a complex beam parameter of $i \cdot 0.401$ and $i \cdot 0.374$ was determined for X and Y respectively. To be able to propagate the beam through the 9.3 meters of total distance from the fibre booster to the 3rd exit pass of AMP1 without clipping or diffraction the beam has to be kept at $< 3.5\text{mm}$ 4sigma beamsize. For simplicity a single lens configuration was found, using a $f=2300\text{mm}$ focal length placed 2300mm from the exit of the booster amplifier, Fig 4.3.5.

single lens arrangement to get through AMP1

$$ls(z, f) := s(z) \cdot l(f)$$

$$prop(z, d1, f1) := \begin{cases} s(z) & \text{if } z \leq d1 \\ ((ls(z - d1, f1) \cdot s(d1))) & \text{otherwise} \end{cases}$$

$$qx(z, d1, f1) := \frac{\left(\begin{matrix} prop(z, d1, f1)_{0,0} \cdot q0x + prop(z, d1, f1)_{0,1} \\ prop(z, d1, f1)_{1,0} \cdot q0x + prop(z, d1, f1)_{1,1} \end{matrix} \right)}{\sqrt{\left(\operatorname{Im} \left(\frac{1}{qx(z, d1, f1)} \right) - 1 \cdot \frac{\pi}{\lambda} \right)^{-1}}}$$

$$qy(z, d1, f1) := \frac{\left(\begin{matrix} prop(z, d1, f1)_{0,0} \cdot q0y + prop(z, d1, f1)_{0,1} \\ prop(z, d1, f1)_{1,0} \cdot q0y + prop(z, d1, f1)_{1,1} \end{matrix} \right)}{\sqrt{\left(\operatorname{Im} \left(\frac{1}{qy(z, d1, f1)} \right) - 1 \cdot \frac{\pi}{\lambda} \right)^{-1}}}$$

$$wxprop(z, d1, f1) := \sqrt{\left(\operatorname{Im} \left(\frac{1}{qx(z, d1, f1)} \right) - 1 \cdot \frac{\pi}{\lambda} \right)^{-1}}$$

$$wyprop(z, d1, f1) := \sqrt{\left(\operatorname{Im} \left(\frac{1}{qy(z, d1, f1)} \right) - 1 \cdot \frac{\pi}{\lambda} \right)^{-1}}$$

f1 := 2290 focal length
d1 := 2300 distance from output of booster amp

$$qx(200, 400, 890) = 200 + 1.117i \times 10^3 \qquad prop(20, d1, f1)_{0,0} = 1$$

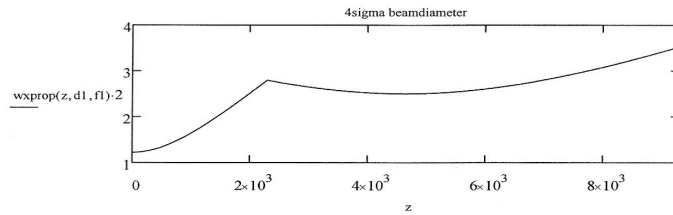


Fig. 4.3.5. Calculated beam propagation to the end of AMP1

An additional $\lambda/2$ plate and a polarizer were installed to set the correct polarization input to AMP1. All alignment references were kept from the previous setup. With this configuration the following power levels were measured through the system, Table 4.3.1.

| Position | Transmission respect to booster output |
|-----------|--|
| AMP1 in | 96.5% |
| AMP1 out | 80.7% |
| AMP2 in | 57% |
| AMP2 out | 48% |
| Before PC | 46.4% |

Table 4.3.1 Transmission through the system

The values corresponded well with previous measurements of the preamp input, confirming that there was no clipping in the amplifiers. The beam was amplified to 1.7kW mean power after AMP1 at 90A pump current, corresponding to 1.1μJ per pulse. However strong over-pumping was observed and so pumping time of AMP1 was reduced to 250μs from the original 400μs. The mean power in this case was 1.6kW.

Conversion was checked to see the ASE content of the signal. 30% conversion efficiency to green was measured and confirmed clean amplification.

For AMP2 the pumping time - according to the change on AMP1- was reduced to 200 μ s. 9.4kW mean power was measured this way with excellent beam profile after AMP2 Fig 4.3.6. This corresponds to 6.3 μ J/ pulse at the exit of the PC.

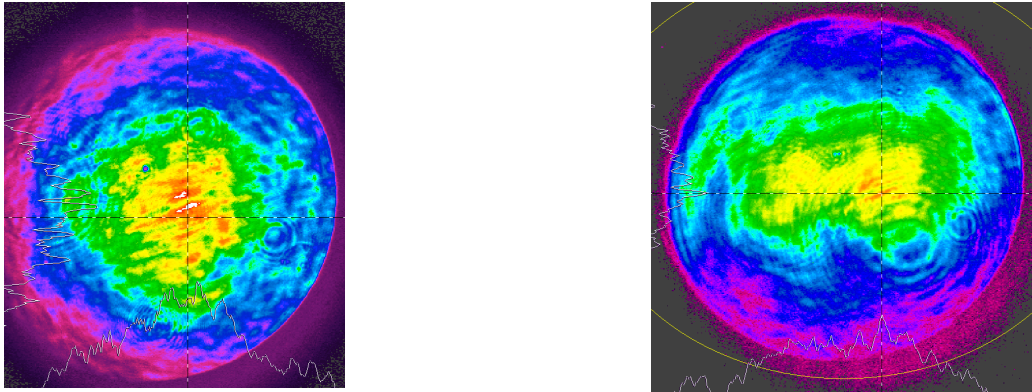


Fig. 4.3.6. Beam profiles after AMP2 with booster amp input at 140mW at AMP1 (left) and with previously used HighQ 7.4W input (right), with same attenuators in front of the camera.

Although mean power levels at the time of the PC switching are comparable with the higher seed input to AMP1 and AMP2, reduced pumping time results in slower build-up of the steady state. Although amplitude stability of the booster seed is higher, than of that of the HighQ preamp, we benefit less from the stabilizing effect of the steady-state saturated amplification in this case. 0.6% RMS stability was measured in the IR, which is only slightly above the 7W seeded case, where 0.35% was the typical value.

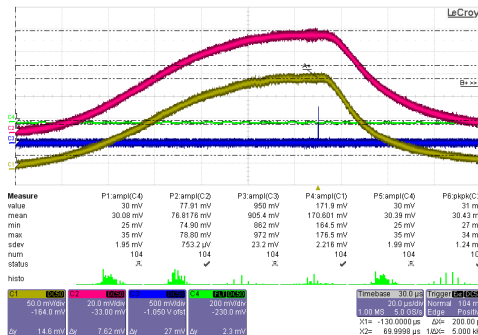
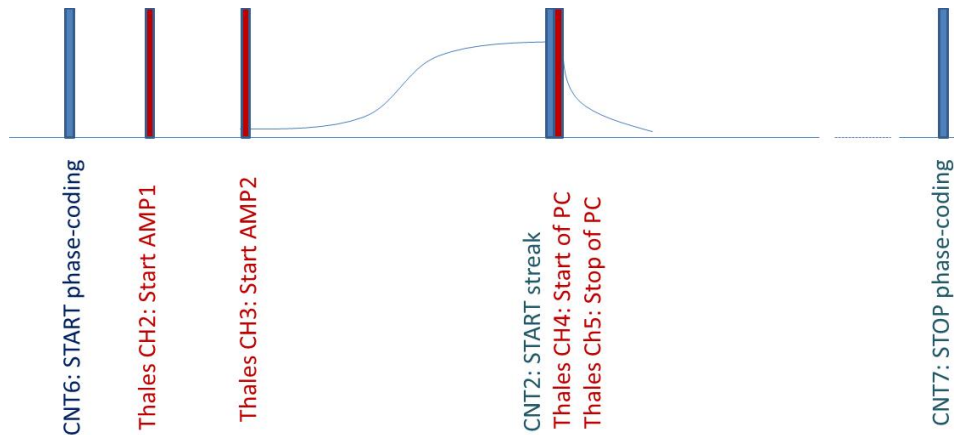


Fig. 4.3.7. Amplification curves showing build-up of steady-state measured with DET10A Thorlabs photodiodes at the exit of each amplifier. Red AMP1, yellow AMP2

With no additional adjustment made to the lens systems in the harmonics stages 710 nJ/ pulse was obtained in the UV, which after transport losses gave a maximum of 450nJ/ pulse on the cathode, well above the 370nJ specification. Conversion efficiencies of 38% and 27% were measured to green and to UV respectively.

4.4 Timing signals for the phase-coding

Once amplification and phase-coding takes place at the same time, timing signal settings become crucial. Switching has to take place, when PC is ON and timing signals are available for streak measurements. We have also found, that the timing quality of the switching signal degrades when it is used ms's after the START and so it is important to amplify and use the phase-coded signal <1ms after the START is given to the modulator drivers.



Red signals come from Thales clock and have 4ns jitter performance
Blue signals come from ECL counters and have 5ps? Jitter performance

Fig.4.4.1: Triggers for phase-coding

5. Measurements with phase-coding

5.1. Measurements on the laser

5.1.1 Timing and amplitude accuracy

Long term amplitude stability measurements were carried out to check performance in the phase-coded and non-phase-coded cases. As with the reduced input to the amplifiers we have less saturation and the overall stability was expected to be worse than during the previous run. A DET10A small area photodiode, sensitive down to 220 nm wavelength was used. The detector is sensitive to beam movement and previous noise floor measurement show $\sim 700\mu\text{V}$ RMS noise. The measured RMS values are expected to be combination of pointing and amplitude error.

No difference between the phase-coded (PC) and non-phase-coded (NPC) cases were observed, Fig 5.1.1.1. Energy integrated over the whole pulse-train in the two cases was also measured with charge stability measurements running parallel, Fig 5.1.1.2. In the phase-coded case the measurement data was not useable for the BPR.

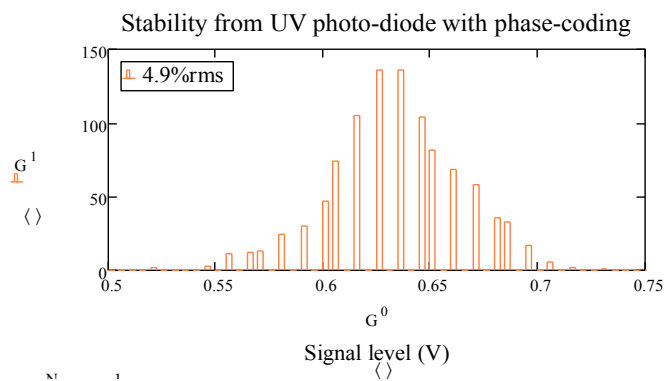
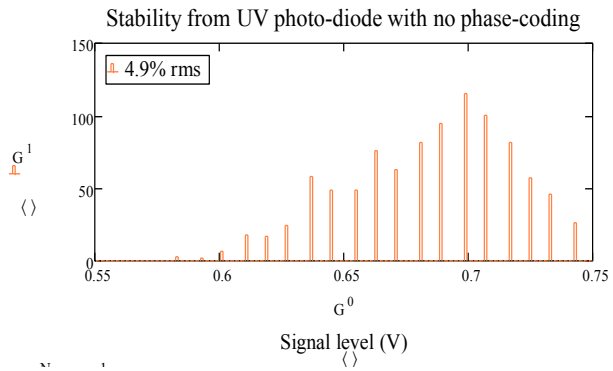
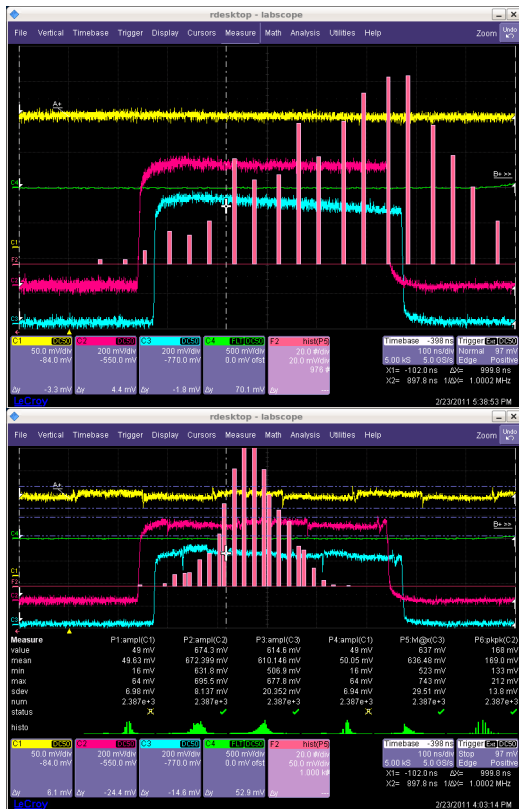


Fig. 5.1.1.1. Micropulse stability at fixed point of the train measured with PD in the UV before beam leaves the laser room.

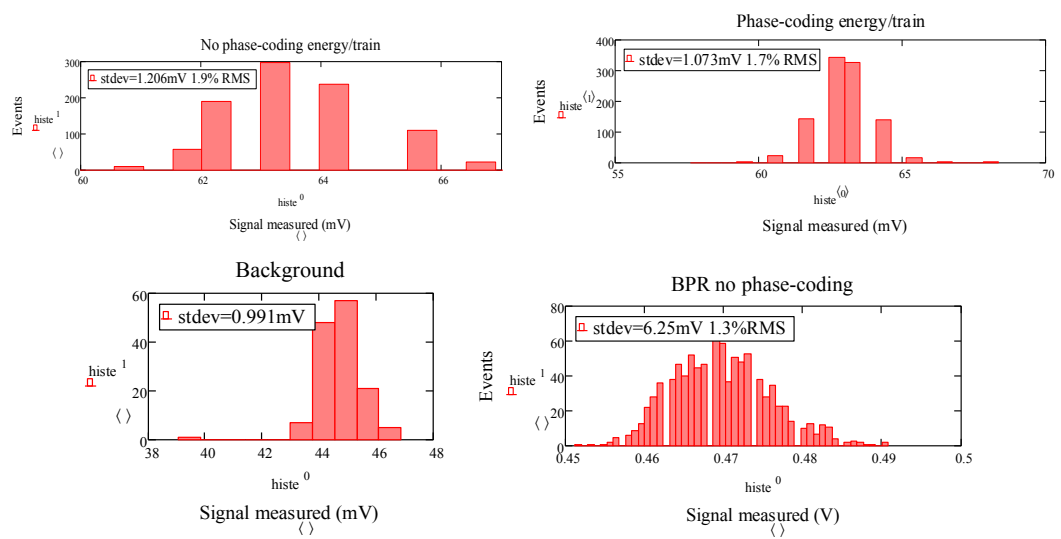


Fig. 5.1.1.2 Macropulse energy stability measurements and parallel charge stability measurement

The laser energy measurement in CTF2 showed the same stability in both the PC and NPC cases and gives an upper limit to the energy stability, as the background noise of the detection system is relatively high ($\sim 1\text{mV}$) with measured values being in the region of $\sim 60\text{mV}$ in this case. BPR measurements show good consistency with the measured $\sim 1.9\%$ RMS at the laser in the NPC case.

Streak camera measurements were carried out directly on the laser to confirm accurate time-delay settings, Fig 5.1.1.3.

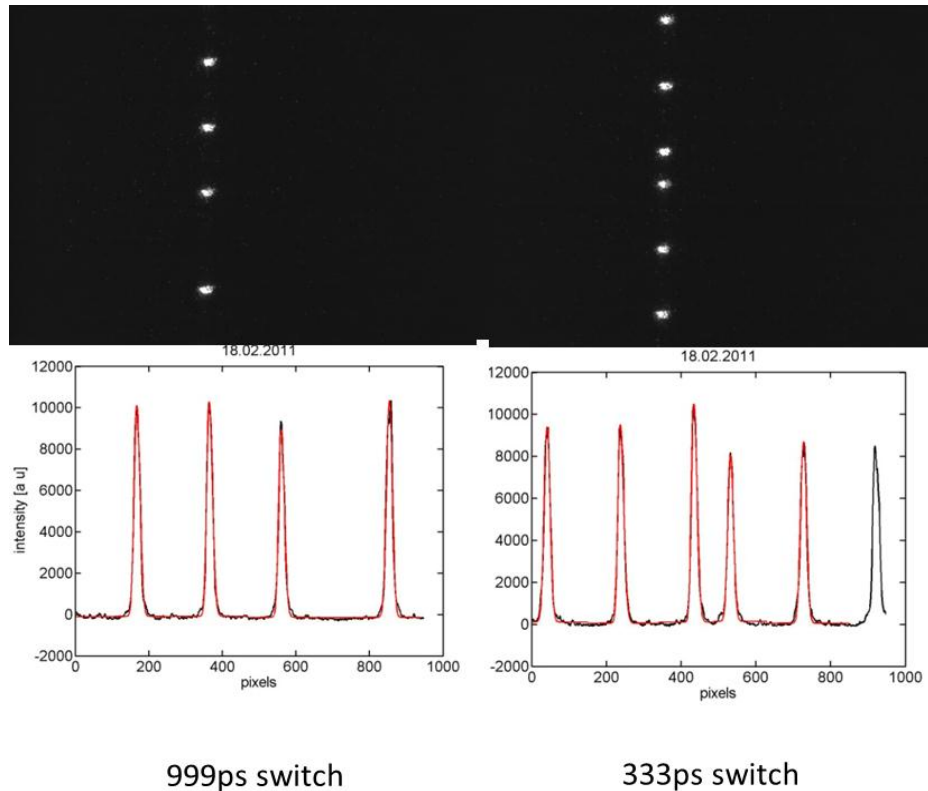


Fig. 5.1.1.3. Measurements performed on the 523nm on the laser system to confirm switching

The pulse separation was within specification and is not expected to drift by more than few 100fs.

5.1.2. Satellite measurements

When a bias drift occurs in the modulators, the extinction ratio between the ON and OFF states gets worse. The ON state signal will drop and in OFF state there will be pulses leaking though as shown in figure 5.1.2.1, resulting in satellites in between the wanted electron bunches. As there was no active stabilization used for the bias this time we were interested to see how these bias errors affected the amplification and later the conversion and electron production. A bias error larger than expected from temperature drifts at 1.5V level was introduced, causing satellites at $\sim 20\%$ level. For illustration the other modulator was kept in a perfect switching state. The satellites on the relative slow detectors will appear as a DC error in the other sub-train. These pulses are conserved and amplified with the same gain as the main pulses. However as these pulses contain very small pulse energy relative to the main pulses during the two non-linear processes the energy in the UV will be only $\sim 5\%$ of the main pulses. To be within the specified 4% for CLIC one would have to make sure; that bias drift are kept below 1V, which given the full switching voltage of 5V is reasonable under normal laboratory conditions.

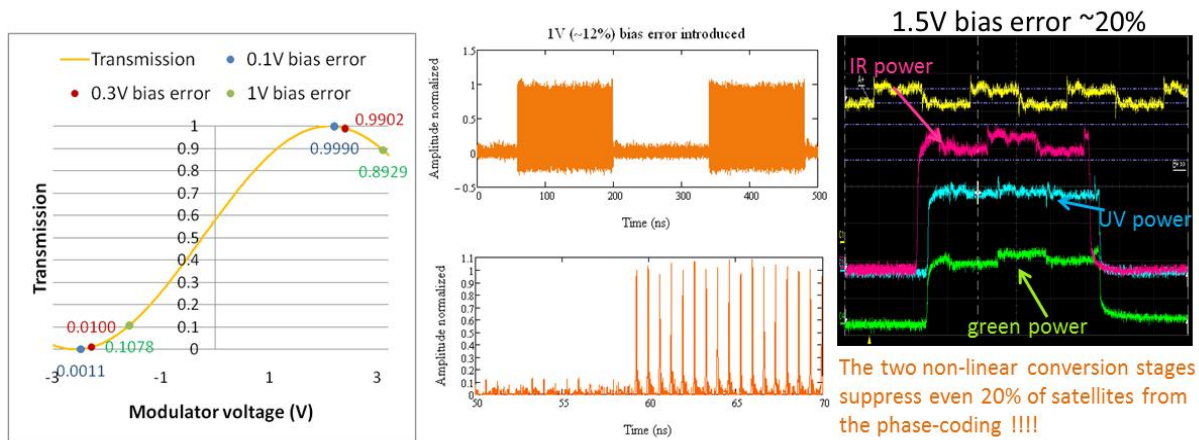


Fig.5.1.2.1 Bias error propagation measurement.

5.2. Measurements on PHIN

5.2.1. Cherenkov-line measurements

The Cherenkov-line was designed in collaboration with BI group, with the aim to resolve bunch-separation and was based on the CTF2 design Fig 5.2.1.1. Solenoid magnets, a steering magnet, and a beam positioning monitor are used to optimize the beam transport to the position of the beam profile monitor. For bunch length measurements a 300 μ m aluminium-coated sapphire Cherenkov-target is used, which generates a flux of visible photons compatible with the sensitivity of the streak camera. OTR, used for transverse profile measurement would have provided better resolution, but with the 5MeV beam then light intensity would not have been sufficient for detection with a streak camera. Detailed design and information can be found:

dfs:\Workspaces\p\PHIN_photoinjector\Cherenkov-line

Optical line to transport line from CTF2 to the laser lab

- ✓ Design of the optical line done with Zemax software in December 2010
- ✓ Construction and alignment of the optical line done in December/January

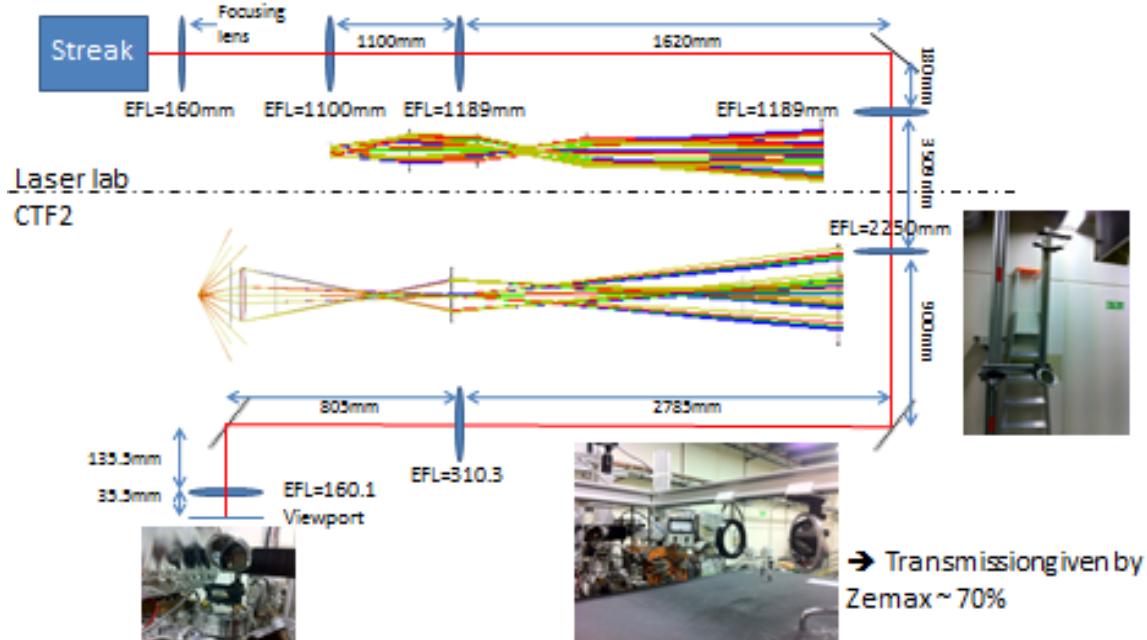


Fig 5.2.1.1: Cherenkov-line layout from CTF2/PHIN to laser room.

a) Time resolution:

The least-time principle will assure that the photons generated by electrons arriving with the same speed at the same time in the same place will also appear at the same time on the exit of the plate. However there is a delay between photons, which were produced by electrons at different speeds and on a different part of the plate. The electrons which propagate through the plate will produce photons both at the entry and the exit surface with a time delay, which is proportional to the relative speed of the electrons and the photons and also to the thickness of the plate. To calculate the time resolution achievable from the plate only, one needs to take into account the path difference between AB and DEFC fig 5.2.1.2. The captured area as a consequence will also affect the time-resolution. It is the best however to capture the whole beam and it is also desirable to have the smallest beam in the emitter plate. With 2mm sigma measured at the focus in PHIN one would expect 11ps time resolution from the plate.

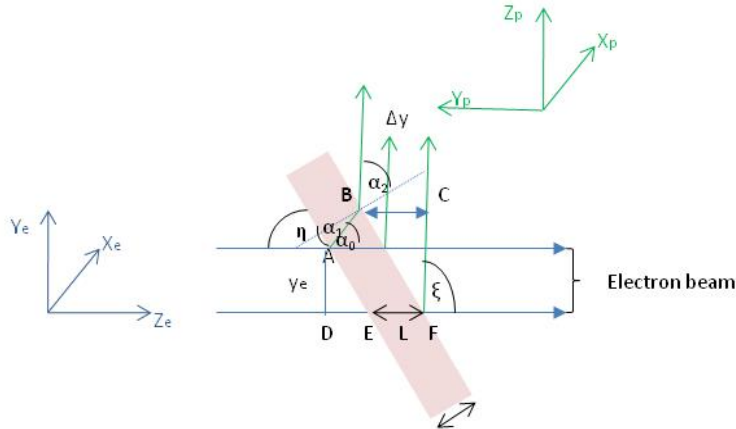


Fig. 5.2.1.2 Geometry of the photon emission from the Sapphire plate

The number of photons produced will depend on the number of electrons, their energy, the thickness of the plate, the spectral range observed and the transverse and angular acceptance of the streak camera. We are expecting $\sim 5 \cdot 10^{-3}$ photons/electron to arrive at the streak camera, which with the 2.3nC nominal charge should be plenty. However we have found, that to have enough light intensity on the streak camera for single bunch measurements the smallest bandwidth filter which could be used to improve resolution was one with $\sim 200\text{nm}$ bandwidth Fig 5.2.1.3.

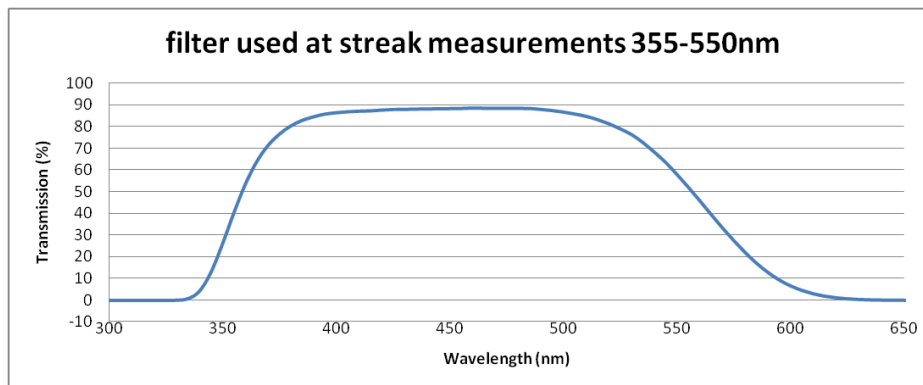


Fig. 5.2.1.3 Bandpass filter used for streak measurements

Dispersion calculations through the transport optics using the spectral width of the filter were done by A. Rabiller. For single bunch measurements, including screen, beam size, streak camera slit acceptance and camera resolution a total resolution of ~ 24 ps was estimated for this set up.

In summary, the single bunch measurement is limited due to:

- Transport optics (total thickness of optics from ZEMAX is 223mm)
- e-beamsize on target
- Thickness of the Sapphire plate
- Light intensity/bandwidth

If there are enough photons produced one could think of using a thinner plate and only taking part of the emitted light too to improve time resolution. Even with an infinitely small electron beam there will always be a residual dispersion due to the difference of speed between the photons and the electrons. The ideal vertical acceptance for transport to keep resolution below 2ps is $\sim 1.5\text{mm}$. Dispersion will also play a role

in the time delay, but with narrow pass filters or reflective optics this could be minimized. However most of these cause loss of photons at the streak camera.

b) Bunch separation measurement:

Taking into account the time resolution of the streak at 250ps/mm sweep speed, the observed bunch separation was within the specification. Amplitude variations over the sub-trains came directly from the laser oscillator, Fig 5.2.1.4.

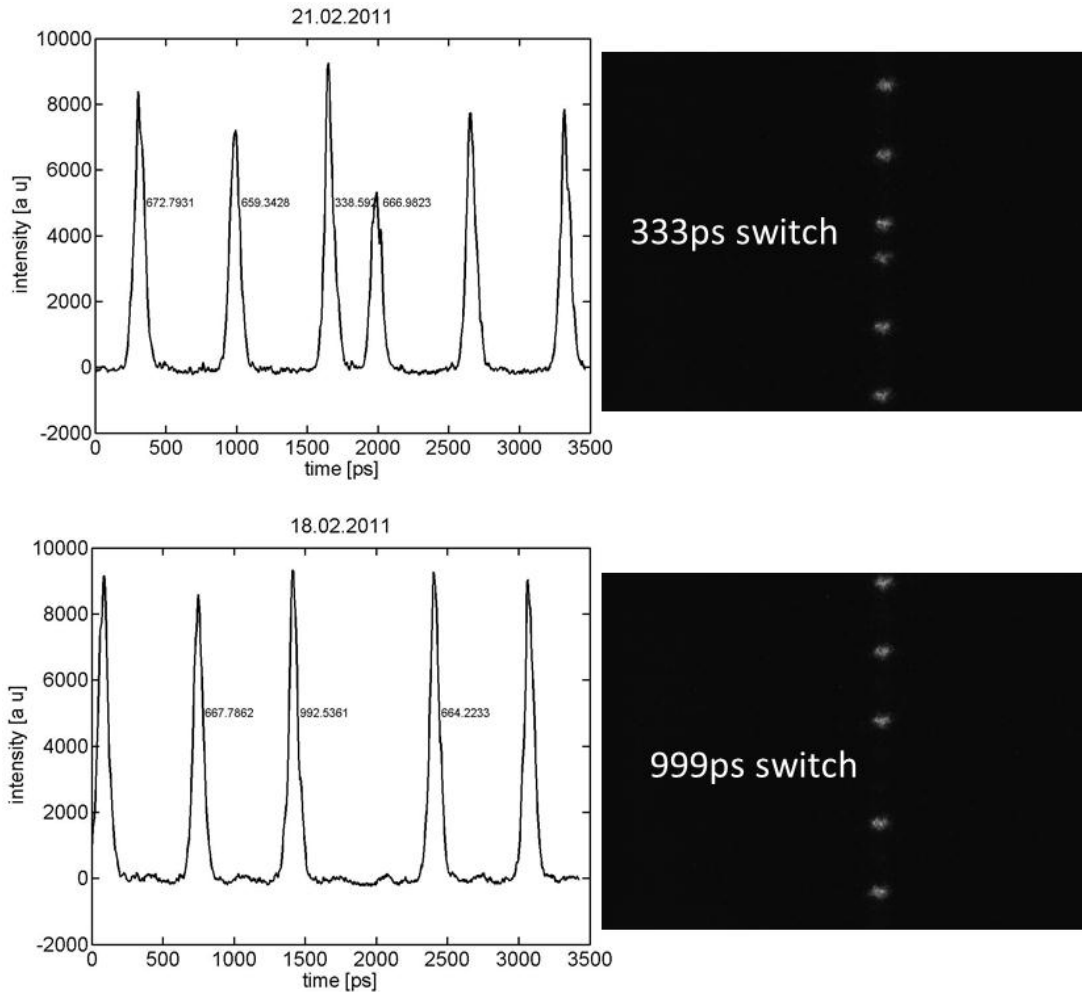


Fig. 5.2.1.4. Bunch separation when switching takes place measured on the streak camera with Cherenkov-light from PHIN

c) Single bunch measurements/ Phase-scan

The first aim was to show, that phase-coding does not have an effect on the bunchlength. Figures below show no difference between phase-coded and non-phase-coded case. The indicated 29ps full width half maximum is not corrected for the time-resolution of the measurement system.

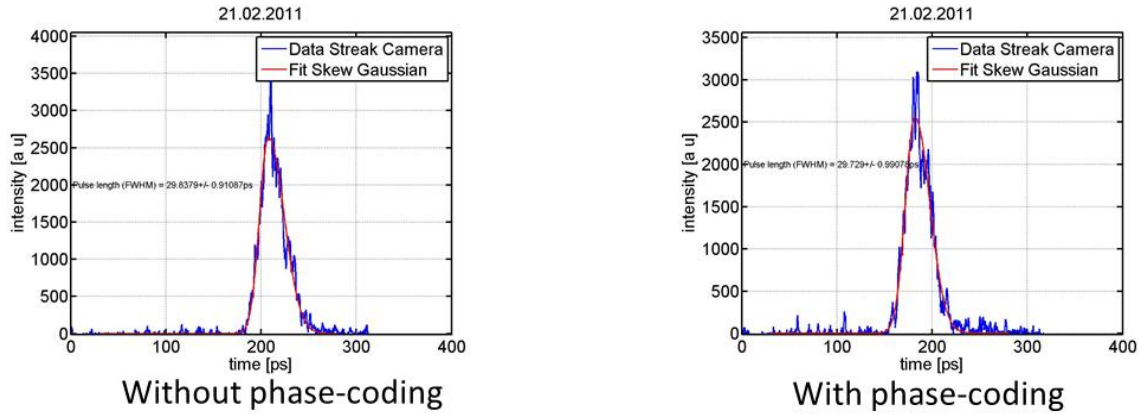
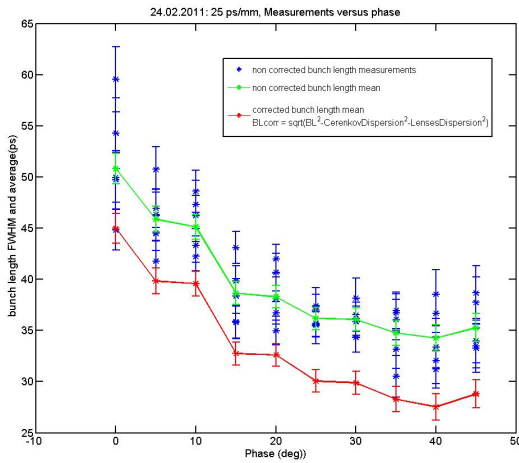


Fig. 5.2.1.5 Single bunch length with and without phase-coding

As Cherenkov-line was available for the first time, a phase-scan was also performed to measure the dependence of the bunch length on phase, Fig 5.2.1.6. The phase is relative to maximum charge phase, moving towards operational phase. Measurements below are corrected for time resolution of the measurement system taking into account the effect of the beam spot size on the crystal and the dispersion of the optical transport. However as it can be seen from the beam size measurement, Fig 5.2.1.7., there was asymmetry in the beam size variation as a function of the phase in X and Y, which makes it difficult to take these variations into account in the calculations.



| Phase (°) | BL (ps) | dBL(ps) |
|-----------|---------|---------|
| 0 | 44.9807 | 1.4655 |
| 5 | 39.8255 | 1.269 |
| 10 | 39.5799 | 1.2125 |
| 15 | 32.7469 | 1.1287 |
| 20 | 32.6185 | 1.0892 |
| 25 | 30.0571 | 1.0915 |
| 30 | 29.8903 | 1.1404 |
| 35 | 28.2737 | 1.2304 |
| 40 | 27.536 | 1.2834 |
| 45 | 28.8041 | 1.3755 |

Fig. 5.2.1.6 Bunch length with correction of beam size and lens thickness as a function of the phase

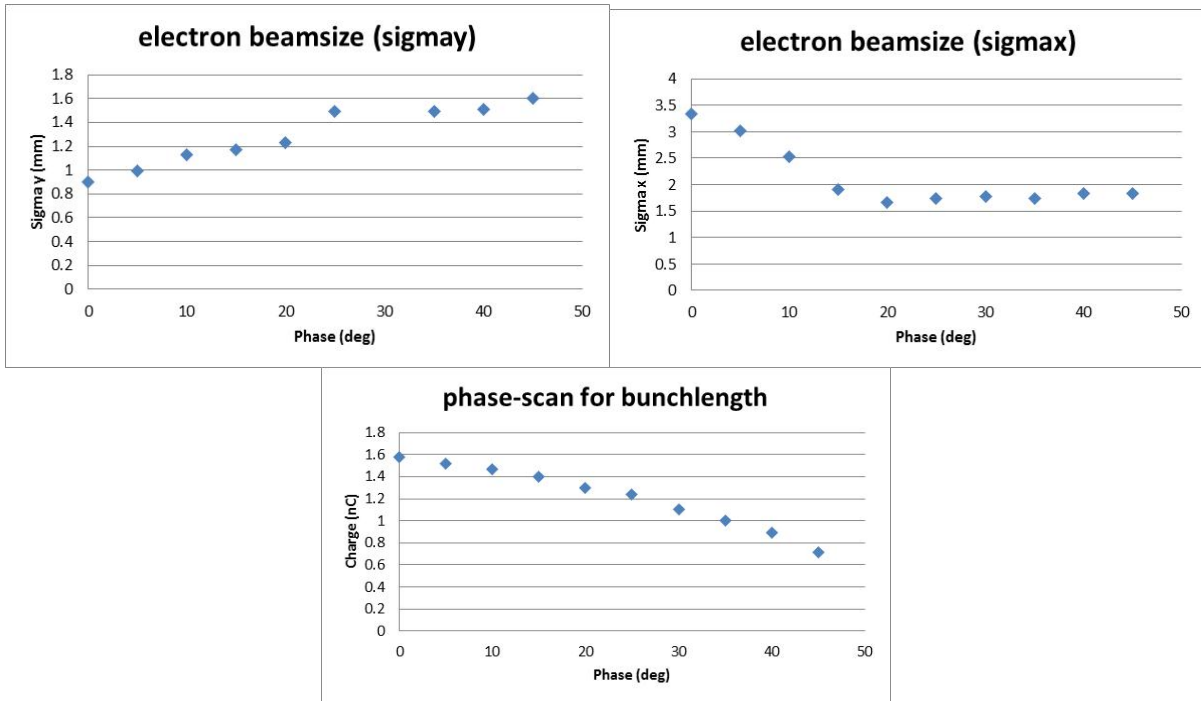


Fig. 5.2.1.7 Electron beam size as function of the phase measured on the OTR screen (top); charge as a function of the phase (bottom)

Simulations were done by O. Mete to see whether the behaviour is as expected, Fig 5.2.1.8. The input parameters for the PARMELA code were taken from the measurements of the laser pulse length with the streak camera and the laser spot size on the virtual cathode camera. The measured data is not consistent with the simulations even after correction for the transport line and the beam spot size.

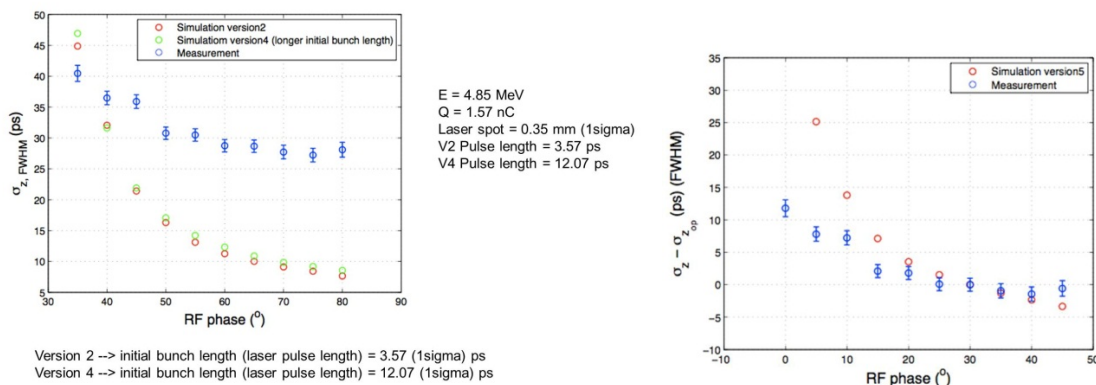


Fig.5.2.1.8 Simulations with different initial pulse lengths and measurement (left); relative bunch lengthening (right)

5.2.2. FCT measurements

A fast current transformer (FCT), installed directly after the gun, is used to monitor the extracted charge. This provides a good tool to check phase and amplitude errors between sub-pulses. The phase error and amplitude imbalance between the laser's sub-pulses appear as a current imbalance between the sub-pulses of the electron pulse. A 10 ps error was introduced in the delay arm of the phase-coding, which

means, that one sub pulse arrives off phase. As shown in Fig. 5.2.2.1, this resulted in a reduction of extracted charge in that sub-pulse, which appears as a DC change with the 30MHz bw filter on the oscilloscope. An amplitude error was also introduced between sub-pulses to check the sensitivity of the FCT, which was found to be <math><1\%</math>. An example with 20% amplitude error is also shown below.

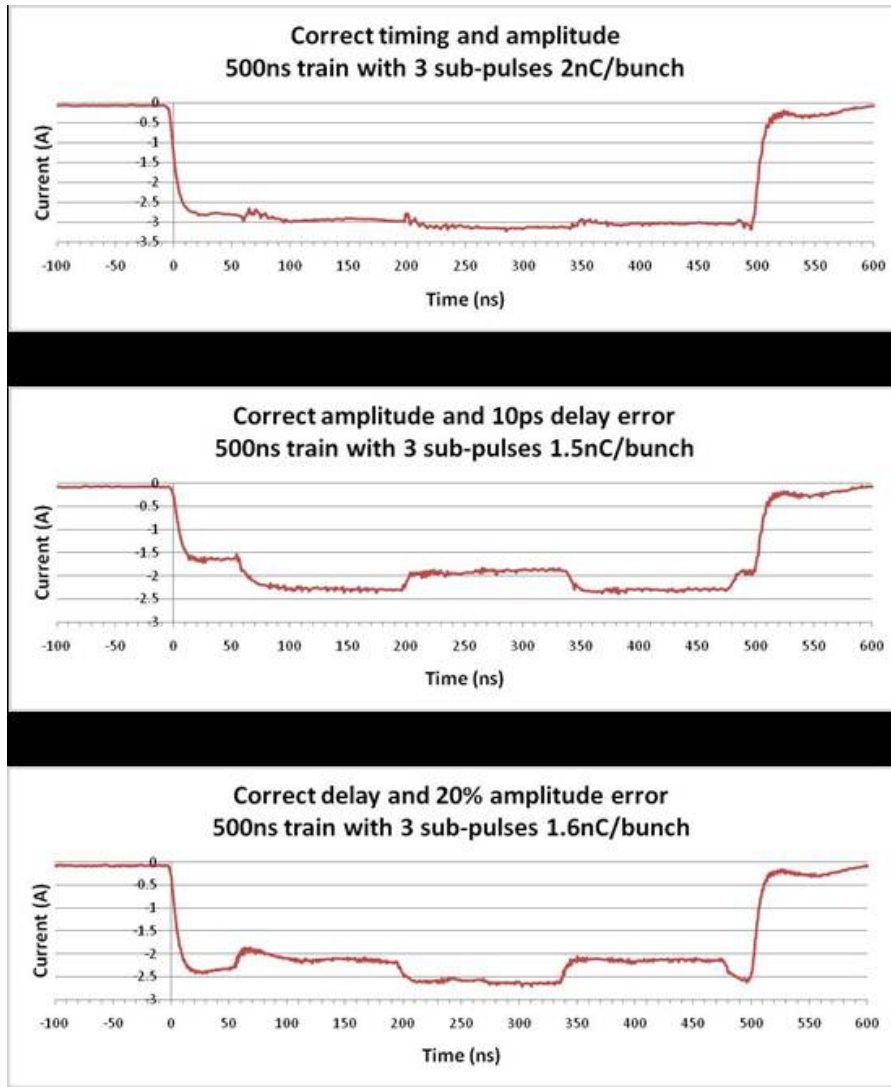


Fig.5.2.2.1 FCT transformer measurements with intentional phase- and amplitude error introduced to the system.

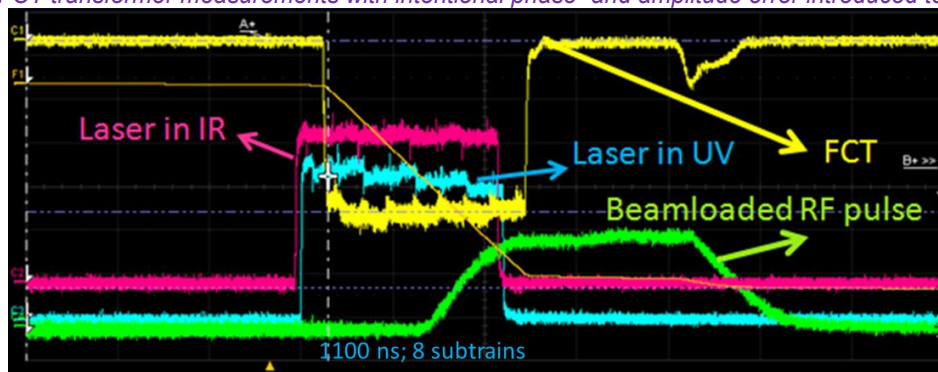


Fig. 5.2.2.2 Phase-coding with nominal parameters, measured on PD's and FCT

5.2.3. Energy measurements

Energy measurements were done with the phase-coded beam to see the difference between subsequent sub-pulses. In all cases a 500ns long train was measured covering two full switches. As during this run one of the aims was to produce high charge, relatively large laser beamsizes were used. As there are no additional optics after the first OTR for transverse measurements this was not in favour of the energy measurements. The beamsize on the OTR dedicated for energy measurements was too big and part of the beam was clipped, some parts supposedly even passed the frame before the segmented dump. Some channels corresponding to these outer parts of the beam were disclosed from the data analysis. Single shot measurements, carried out with segmented dump, therefore were not so successful. Dipole scans were performed measuring momentum evolution along the pulse, each step is integrated over a 20 ns window, Fig 5.2.3.1. Note that the momentum spread also includes the intrinsic size of the beam, which with our case was quite significant.

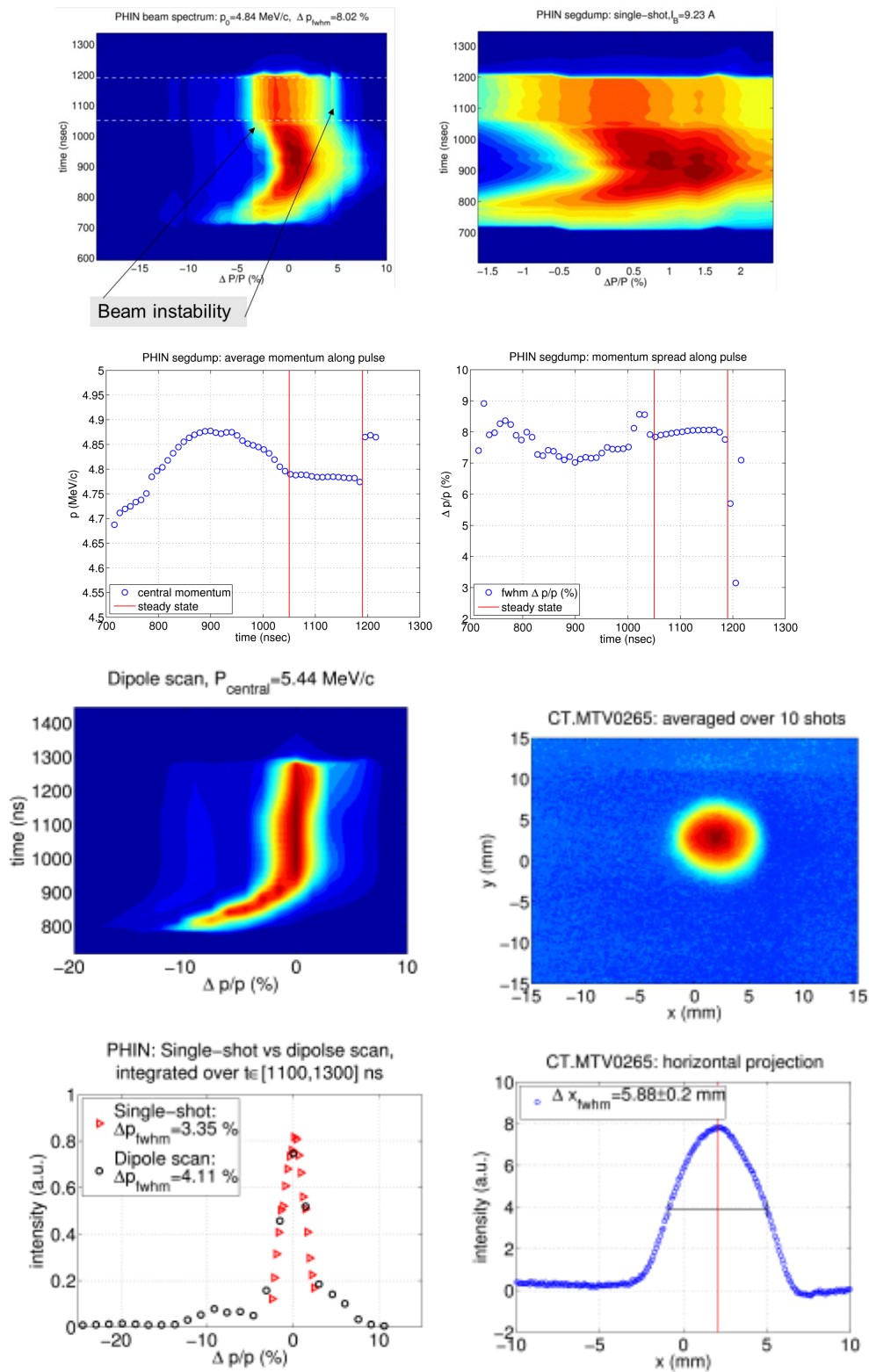


Fig.5.2.3.1 Dipole scan (top left), single shot measurement (top right); no phase-coding and smaller beam (bottom)

Beam instability and beamsizes was limiting our measurement accuracy and although a 140 ns initial step can be seen at the end of the pulse, we are not sure, that this corresponds to the switching of the phase-coding, as one would expect the same behaviour at the beginning of the pulse too.

To see more dramatic effect we have introduced an amplitude and consequently charge imbalance between the sub-trains/ sub-pulses. Again a time-structure similar to that of the phase-coding can be seen on the time resolved energy scan, but the difference between balanced- and unbalanced case are not as significant as expected, Fig 5.2.3.2. RF pulses were unfortunately not recorded this time to be able to tell, whether these variations really came from the phase-coding or RF variation along the pulse, as it was observed before [12].

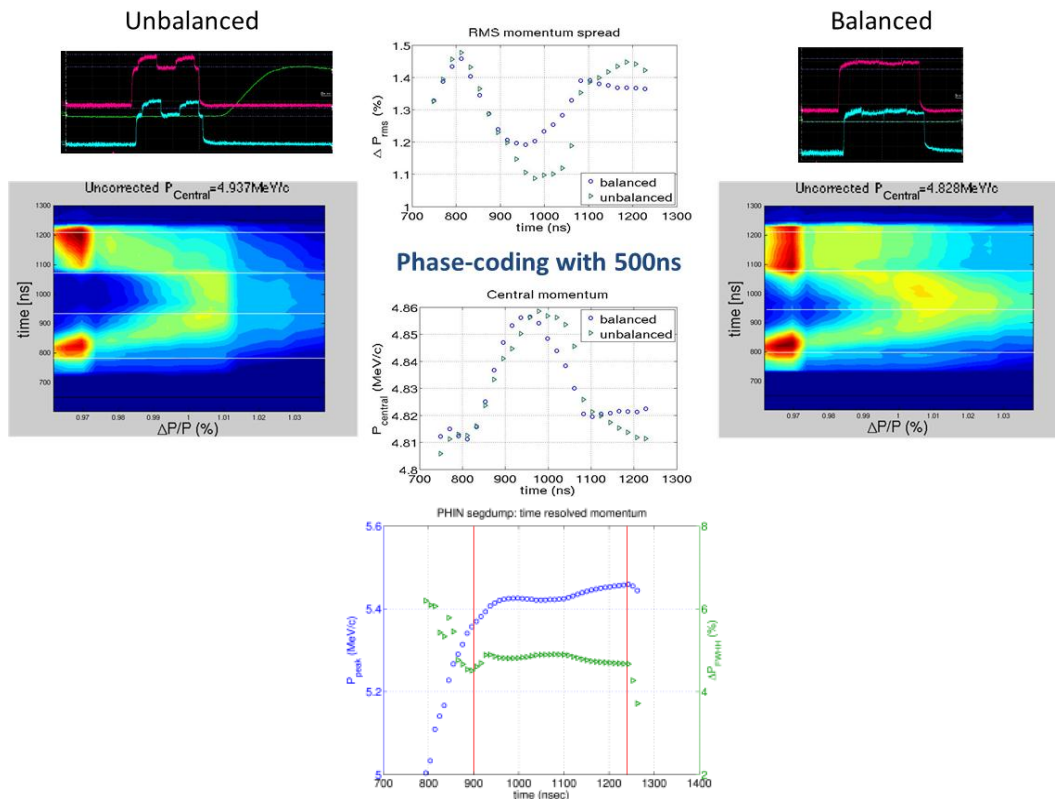


Fig.5.2.3.2 Energy measurement using dipole scan with balanced and unbalanced phase-coding

M. Olvegaard carried out the measurements and analysis and concluded that for absolute values regarding energy and energy spread the following needs to be taken into account:

- We measured the beam size on the screen before the dipole, but this is not sufficient for the prediction of the beam size at the segmented dump.
- The horizontal width was kept constant within <5 %.
- The horizontal position showed a 15 % variation from shot to shot.
- Without a detailed knowledge of the beam emittance and divergence we can only make a rough estimate of the effect of the intrinsic beam size.

More detailed measurements with better matched beamsizes and solenoid setup would improve these measurements. It would also be useful to carry out the same measurements under the same conditions without phase-coding.

5.2.4. Emittance and beam size measurements

Similar time-resolved measurements were also carried out at the first OTR, to see the effect of phase-coding, if any, on the beamsizes and transverse emittance. Details on the methods used for this measurement can be found in Ref [13]. Here we integrated over the central 100ns of each sub-pulse. In parallel, laser beamsizes measurements were taken over the 3 consecutive sub-pulses in the 500ns long pulse Fig 5.2.4.1. Variations were within the measurement errors and have shown no change between balanced, un-balanced and non-phase-coded beam cases.

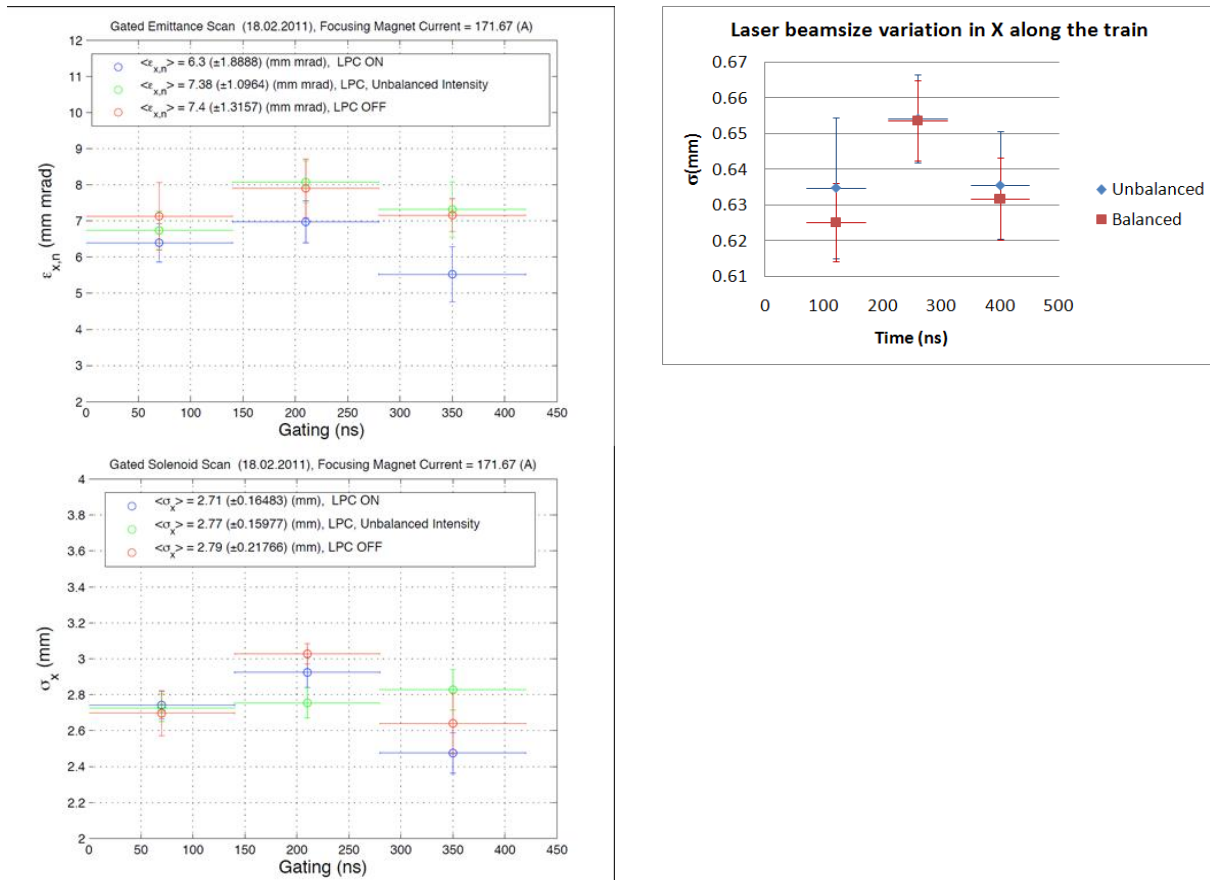


Fig. 5.2.4.1 Emittance measurements over three consecutive sub-pulses using 100ns gating time.

6. Future improvements

On the laser side, a fibre booster amplifier to bring the laser power up to the 10W level after phase-coding would ensure more stable operation.



Fig. 6.1 Scheme with fiber booster at 10W

On the phase-coding system side: To increase transmission through the phase-coding system, all FC/APC connector losses could be suppressed by fusing the fiber components together, which would give a 20% increase in the output power. Active control of the amplitude balance between the two arms via a waveplate- and polarizer-based remotely controlled attenuator could compensate for long-term temperature drifts, and would provide a finer and more reliable attenuation. The modulators themselves could be temperature-stabilized to $\sim 40^{\circ}\text{C}$ to ensure that any drift is minimized. The bias controller for Mod1 should be replaced with a newer model, with finer bias voltage settings.

For ease of measurement and operation dedicated timing signals (counters) for start and stop of phase-coding would be essential.

Purchase of fast UV detectors would allow us to characterise the laser without performing lengthy and complicated streak measurements.

7. Conclusion

Fast phase-switching within the 1.5GHz electron trains was demonstrated on the PHIN photo-injector. The switching is achieved by direct manipulation of the laser pulse structure. The phase-switch can be set with 0.1ps accuracy and introduces no additional jitter to the laser oscillator, which is locked to the 1.5GHz RF frequency with accuracy $< 500\text{fs}$. The amplitude balance between sub-trains can be set to the required accuracy of 0.1% rms, and is currently limited by fast noise of the laser oscillator. Emittance, energy and stability measurements show no measureable beam degradation due to the phase-coding. Some long term drift measurements could be performed in the future with improved drift controls on the laser side. Energy measurements with full recording of the RF and beam parameters and with optimized beam on the spectrometer screen would compliment the measurements so far. Improved resolution on the Cherenkov-line could provide a useful tool for single bunch measurement studies in the future.

The PHIN photo-injector is the alternative to the thermionic source for CLIC test facility 3, where sub-harmonic bunching and fast RF phase-switching are used to generate the required electron bunch structure for frequency multiplication. The photo-injector, with the fibre-optic modulator-based switching system, would significantly improve radiation and efficiency losses for the 1.5-12GHz beam combination in CTF3, and would also provide a solution for the future CLIC machine.

References

- [1] C.P.Welsch et al., Longitudinal beam profile measurements at CTF3 using a streak camera, 2006 JINST 1 P09002
- [2] P.Urschütz et al., Beam dynamics and first operation of the sub-harmonic bunching system in the CTF3 injector, Proceedings of EPAC, Edinburgh, Scotland, (2006), pp. 795
- [3] A. Masi 'Report on the visit to the 2005 Pulsed Power Conference' CERN-AB-2004-001 GGG
- [4] www.versawave.com
- [5] Ed L Wooten et al., A Review of Lithium Niobate Modulators for Fiber-Optic Communication Systems, IEEE Journal of Selected Topics in Quantum Electronics, Vol.6. No.1. (Jan 2000), p69.
- [6] F.J.Leonberger, High-speed operation of LiNbO3 electro-optic interferometric waveguide modulators, Opt. Lett., Vol.5., No.7. (1980) pp.312
- [7] www.photoline.com (Herve Gouraud)
- [8] G.Kurdi et al., Development of the CTF3 photo-injector laser system, STFC CLF annual report (2007) pp. 225
- [9] I. Boscolo, S. Cialdi, D. Cipriani and F. Castelli, CERN-CTF3 Laser Phase Coding System and Tests, October 26, 2007 (EDMS number??)
- [10] M. Csatari Divall et al., Fast phase switching within the bunch train of the PHIN photo-injector at CERN using fiber-optic modulators on the drive laser NIMA53834 Nucl. Instr. and Meth. Phys. Res. A
- [11] S. Battisti: Measurement of the short bunch length in the CLIC Test Facility CTF CERN-PS 93-40 BD
- [12] D. Egger et al. Design and Results of a Time Resolved Spectrometer for the 5MeV Photo-injector PHIN IPAC2010
- [13] Ö. Mete, E. Chevally, A. Dabrowski, M. Divall, S. Döbert, D. Egger, K.Elsener, V. Fedosseev, T. Lefèvre, M. Petrarca, CLIC-Note-809 (2010) <http://cdsweb.cern.ch/record/1262856/files/CERN-OPEN-2010-013.pdf?version=1>